Microtubule-dependent intracellular trafficking promotes apical constriction during tissue invagination

Thao Phuong Le[1] and SeYeon Chung[1, *]

[1] Department of Biological Sciences, Louisiana State University, Baton Rouge, LA 70803, USA

[*]Author for correspondence: seyeonchung@lsu.edu

Abstract

The formation of an epithelial tube is a fundamental process for organogenesis. During *Drosophila* embryonic salivary gland (SG) invagination, Folded gastrulation (Fog)-dependent Rho-associated kinase (Rok) promotes contractile apical myosin formation to drive apical constriction. Microtubules (MTs) are also crucial for this process and are required for forming and maintaining apicomedial myosin. However, the underlying mechanism that coordinates actomyosin and MTs networks is still unclear. Here, we show that MT-dependent intracellular trafficking regulates apical constriction during SG invagination. Key components involved in protein trafficking, such as Rab11, Nuclear fallout (Nuf) and dynein heavy chain, are apically enriched near the SG invagination pit in a MT-dependent manner. Disruption of the MT networks or intracellular trafficking impairs apicomedial myosin formation and apical constriction. We show that MTs and dynein motors regulate Fog signaling activity. We further show that Rab11-dependent protein transport along MTs mediates clustered apical constriction during SG invagination. Key proteins that are transported include the apical determinant protein Crumbs (Crb), the key adherens junction protein E-Cadherin (E-Cad) and the scaffolding protein Bazooka/Par3. Targeted knockdown of these genes in the SG disrupts apical myosin networks and results in apical constriction defects. These results define a role of MT-dependent intracellular trafficking in regulating actomyosin networks and cell junctions, to coordinate cell behaviors during tubular organ formation.

Introduction

Formation of three-dimensional tubes by invagination of flat epithelial sheets is a fundamental process in forming organs such as the lungs and kidneys (Andrew and Ewald, 2010). To enter the third dimension, cells must change their shapes and positions relative to each other. A major cellular process during epithelial tube formation is apical constriction, a universal cell shape change that is linked to tissue bending, folding and invagination (Martin and Goldstein, 2014; Sawyer et al., 2010). During apical constriction, the apical side of an epithelial cell constricts, causing a columnar or cuboidal cell to become wedge-shaped (Martin and Goldstein, 2014; Sawyer et al., 2010). Manipulation of apical constriction in a group of cells impacts both local and global tissue shape directly, suggesting a critical role for apical constriction in forming proper tissue architecture (Chung et al., 2017; Guglielmi et al., 2015; Izquierdo et al., 2018).

Apical constriction is driven by actin filament (F-actin) networks and the molecular motor non-muscle myosin II (hereafter referred to as myosin). Over the past decade, important functions of different actomyosin structures in epithelial tissue morphogenesis have been discovered. Particularly, studies in *Drosophila* revealed a distinct population of pulsatile apical medial actomyosin (hereafter referred to as apicomedial myosin) that generates a pulling force that exerts on adherens junctions to drive apical constriction (Booth et al., 2014; Chung et al., 2017; Martin et al., 2009; Rauzi et al., 2010). In early *Drosophila* embryos, apicomedial myosin is created in response to signaling by the Folded gastrulation (Fog) ligand and its G protein-coupled receptors (GPCRs) (Kerridge et al., 2016; Manning et al., 2013), and is regulated by apical Rho-associated kinase (Rok) (Mason et al., 2013). Apical junctions and apical determinants also have an important role in the formation of functional actomyosin complexes. During *Drosophila* dorsal closure, the apical polarity regulators Par-6, aPKC and Bazooka/Par3 (Baz/Par3) (altogether known as the Par complex) regulate pulsed actomyosin contractions in amnioserosa cells (David et al., 2010). In the *Drosophila* embryonic trachea, the apical protein Crumbs (Crb) is required for proper organization of the actomyosin complex (Letizia et al., 2011).

72 Emerging evidence suggests that microtubules (MTs) play a critical role in tissue
73 invagination (Booth et al., 2014; Ko et al., 2019). MTs serve as tracks in intracellular
74 transport, raising the possibility that MTs regulate apical constriction through the endo-
75 and exocytosis of membrane receptors and adhesion molecules (Khanal et al., 2016; Le
76 Droguen et al., 2015). Several lines of evidence suggest the importance of the endocytic
77 pathway, including the molecular motor dynamin and the vesicle trafficking Rab proteins,
78 in apical constriction in both in vitro and in vivo systems. During *Xenopus* gastrulation,
79 disrupting endocytosis with dominant-negative dynamin or Rab5 perturbs apical
80 constriction and invagination of cell sheets (Lee and Harland, 2010). During *Drosophila*
81 gastrulation, the apical surface of cells is reshaped via Rab35 and RabGEF Sbf, which
82 direct the plasma membrane to Rab11-positive recycling endosomes through a dynamic
83 interaction with Rab5 endosomes to reshape actomyosin networks (Miao et al., 2019).
84 Moreover, in the developing neural tube in *Xenopus*, asymmetric enrichment of Rab11 at
85 the medial apical junctions is critical for apical constriction, suggesting that membrane
86 trafficking has a key role in apical constriction (Ossipova et al., 2014). However, exactly
87 how membrane trafficking, MTs, and actomyosin networks are linked remains to be
88 discovered.

89 To determine how these three cellular attributes contribute to tissue invagination, we use
90 the *Drosophila* embryonic salivary gland (SG) as a model. We and others showed that
91 apical constriction is regulated in a highly coordinated and spatiotemporally controlled
92 manner during epithelial tube formation (Booth et al., 2014; Chung et al., 2017; Myat and
93 Andrew, 2000; Sanchez-Corrales et al., 2018). The *Drosophila* embryo forms two SG
94 tubes via invagination of two epithelial placodes on the ventral surface (Chung et al.,
95 2014). Before invagination, a small group of cells in the dorsal/posterior region of each
96 SG placode begin to constrict. As those cells internalize to form the invagination pit, more
97 cells anterior to the pit undergo clustered apical constriction in a Fog signaling-dependent
98 manner (Chung et al., 2017) (Fig. 1A). In the absence of *fog*, SG cells fail to accumulate
99 Rok and myosin in the apicomedial region of the cells. MTs aid in the formation and
100 maintenance of the apicomedial myosin network during SG invagination (Booth et al.,
101 2014). The MT cytoskeleton near the invagination pit forms a network of longitudinal MT
102 bundles, with the minus ends of MTs facing the apical domain of the cells and interacting

with the apicomedial myosin (Booth et al., 2014). Disruption of MTs causes loss of apicomedial myosin and disrupted apical constriction during SG invagination (Booth et al., 2014). However, it is still unknown how intracellular trafficking affects these two processes.

In this study, we demonstrate that key proteins involved in intracellular trafficking - including Rab11, its binding partner Nuclear fallout (Nuf), and dynein heavy chain - are enriched in the apical domain of SG cells during invagination. Moreover, this accumulation is MT-dependent. Our data suggest that apical transport of several proteins, including the apical determinant protein Crb, the key adherens junction protein E-Cadherin (E-Cad), and the scaffolding protein Baz/Par3, is compromised when the MT networks are disrupted. We further show that disruption of MTs or reducing dynein heavy chain leads to a decrease of Rok and myosin in the apical domain and causes uncoordinated apical constriction in the SG. Altogether, our work mechanistically links MT-dependent intracellular trafficking to the regulation of actomyosin networks during tubular organ formation.

Results

Intracellular trafficking components are apically enriched near the invagination pit

To test a role for the intracellular trafficking machinery in spatially biased signaling activation and protein accumulation during SG invagination, we analyzed the subcellular localization of proteins that are involved in vesicle trafficking in the SG. Several endosome markers were tested, including Rab5 (an early endosome marker) (Gorvel et al., 1991), Rab7 (a late endosome marker) (Meresse et al., 1995; Wichmann et al., 1992), Rab11 (a recycling endosome marker) (Ullrich et al., 1996), Nuclear fallout (Nuf, a putative binding partner for Rab11) (Riggs et al., 2003), and Sec15 (an exocyst complex component and effector for Rab11) (Langevin et al., 2005; Zhang et al., 2004). We observed enrichment of Rab11, Nuf, and Sec15 at and near the SG invagination pit, suggesting active trafficking activities in the region where cells are apically constricting (Figs. 1C-D', G-H';

131 Sup. Figs. 1F-H). Using labeling with E-Cad, an adherens junction marker, and CrebA, a
132 SG nuclear marker, we segmented apical cell outlines (Figs. 1B, B'). Intensity mean of
133 Rab11 or Nuf in the apical domain of each cell showed a negative correlation with the
134 apical area of cells in the entire SG (Fig. 1E), further supporting the conclusion that
135 increased trafficking and apical constriction are closely linked.

136 Rab5, an early endosome marker, was also upregulated near the invagination pit,
137 suggesting active endocytosis in this region (Figs. S1B and B'). Dynein heavy chain, a
138 subunit of the dynein motor complex that transports cargos along MTs toward their minus
139 ends, also showed upregulation near the invagination pit (Figs. 1J and J'). Rab7, a late
140 endosome marker, however, did not show any enrichment but localized as large punctate
141 structures in the cytoplasm of the entire SG placode (Figs. 1L and L'), suggesting that
142 trafficking from early to late endosomes or between late endosomes to lysosomes is not
143 upregulated near the pit during SG invagination. Overall, our results suggest active
144 intracellular trafficking, possibly both endo- and exocytosis, near the invagination pit
145 during SG invagination.

146

147 **MT-dependent vesicular transport is required for apical constriction in the SG**

148 Strong apical enrichment of Rab11 and Nuf in the SG cells near the invagination pit led
149 us to test whether these vesicle markers are associated with vertically aligned MTs that
150 could facilitate their polarized distribution. As in many epithelial cells, MT minus- and plus-
151 ends face the apical and the basal domain of the SG cells, respectively (Booth et al.,
152 2014; Myat and Andrew, 2002). Indeed, co-immunostaining of tyrosinated α-tubulin, a
153 marker of dynamic or newly polymerized MTs, and Rab11 showed a partial overlap of the
154 two proteins at the apical region of the SG cells (Figs. 2A'-B''). Mander's overlap
155 coefficients of Rab11 and tyrosinated α-tubulin revealed that 59% of Rab11 signals
156 overlapped with tyrosinated α-tubulin labeling and 34% of tyrosinated α-tubulin signals
157 co-localized with Rab11 signals (Fig. 2C).

158 To test whether Rab11 apical enrichment in SG cells is dependent on MT networks, we
159 disrupted MTs in the SG by overexpressing spastin, a MT-severing protein (Sherwood et
160 al., 2004), using the SG-specific *fkh-Gal4* driver. In control SGs, tyrosinated α-tubulin and
161 acetylated α-tubulin, a marker of stable and longer-lived MTs (Westermann and Weber,
162 2003), were observed abundantly in the apical domain of cells in the whole placode (Figs.
163 2D'',D'''). When spastin was overexpressed in the SG, both tyrosinated and acetylated α-
164 tubulin signals were strongly reduced, revealing loss of MT filaments (Booth et al., 2014)
165 (Figs. 2E'',E'''); the normal upregulation of Rab11 near the invagination pit (Fig. 2D') was
166 also abolished (Figs. 2E',F'). Quantification of Rab11 localization showed that SGs with
167 disrupted MTs showed much lower intensity in the apical domain near the invagination pit
168 compared to control SGs (Fig. 1C' versus Fig. 2G'). Similar patterns were observed for
169 Nuf (Figs. 2F-H). These data suggest that MT networks are required for apical enrichment
170 of Rab11 and Nuf during SG invagination.

171 We next asked if specific modulation of Rab11 levels could compromise apical
172 constriction. To test this possibility, we disrupted the function of Rab11 by overexpressing
173 a dominant-negative form of Rab11 (Rab11S25N-YFP; hereafter referred to as Rab11-
174 DN) in the SG. Compared to controls (Fig. 3A), SGs overexpressing Rab11-DN showed
175 more cells with larger apical area (Fig. 3B,F), suggesting a role for Rab11 in apical
176 constriction during SG invagination.

177 As dynein heavy chain was also enriched near the invagination pit (Figs. 1J,J''), we
178 hypothesized that dynein motors may traffic key proteins along MTs to control apical
179 constriction during SG invagination. Indeed, zygotic knockdown of *Dynein heavy chain*
180 *64C* (*Dhc64C*) in the SG resulted in more cells with larger apical areas during
181 invagination, suggesting defective apical constriction (Figs. 3C,C',F). Since *Dhc64C* has
182 strong maternal expression and is essential for oogenesis and early embryo development
183 (Li et al., 1994), we tried to reduce Dhc64C levels still further by knocking down *Dhc64C*
184 both maternally and zygotically, using a maternal driver *matα-Gal4* along with the SG-
185 specific *fkh-Gal4*. Embryos with reduced maternal and zygotic pools of Dhc64C showed
186 a range of morphological defects in the entire embryo, some of which were severely
187 distorted (data not shown). In embryos with more subtle morphological defects, SG cells

still invaginated and formed a tube. However, SGs showed a range of phenotypes, from relatively normal but with slightly larger apical areas in individual cells (Fig. 3G; mild), to an enlarged invagination pit (Fig. 3G; intermediate), to quite distorted (Fig. 3G; severe).

Klarsicht (Klar), the *Drosophila* Klarsicht-Anc-Syne Homology (KASH) domain protein, mediates apical transport in the SG (Myat and Andrew, 2002) via the MT motor cytoplasmic dynein (Gross et al., 2000). We therefore predicted that *klar* would also influence apical constriction during SG invagination. Indeed, *klar* mutant embryos showed SGs with mild apical constriction defects compared to wild type controls (Figs. 3D-E',F). Overall, our data suggest essential roles of Rab11 trafficking and MT- and dynein-dependent transport in regulating apical constriction during SG invagination.

Compromised intracellular trafficking leads to failure in accumulation of apicomedial Rok and reduction of apicomedial myosin formation in SG cells

The apicomedial myosin structure generates the pulling force to drive apical constriction in SG cells (Booth et al., 2014; Chung et al., 2017), and spastin overexpression inhibits formation of apicomedial myosin during SG invagination (Booth et al., 2014). We therefore tested whether apicomedial myosin formation is affected in SG cells when dynein-dependent transport is compromised. In control SGs, sqh-GFP (a functional GFP-tagged version of the myosin regulatory light chain) (Royou et al., 2004) showed a strong apicomedial myosin web in constricting cells near the invagination pit (Figs. 4A-A''''). Knockdown of *Dhc64C* caused a significant reduction of apicomedial myosin (Figs. 4B-B'''' and C), suggesting its role in forming and/or maintaining apicomedial myosin.

Consistent with previous studies (Chung et al., 2017; Roper, 2012), a myosin pool that is closely associated with adherens junctions, junctional myosin, also showed strong signals in wild type SG cells, often with stronger signals at vertices (Fig. 4A-A'''). Intriguingly, the intensity of junctional myosin was also reduced upon *Dhc64C* knockdown (Fig. 4B-B''' and C). The ratio of apicomedial to junctional myosin was significantly reduced in *Dhc64C* RNAi SGs (Fig. 4C), suggesting a more significant effect on apicomedial than on

junctional myosin upon *Dhc64C* knockdown. Similar to *Dhc64C* knockdown, reduction of apicomedial and junctional myosin was observed in *klar* mutant SGs (Figs. 4D-F). Our data suggests that defective apical constriction in *Dhc64C* RNAi and *klar* mutant SGs could be due to failure in proper organization of myosin structures, primarily in the apicomedial region of SG cells.

We previously showed that Fog signaling-dependent accumulation of apical medial Rok is required for apicomedial myosin formation for coordinated apical constriction in SG cells (Chung et al., 2017). To test whether Rok accumulation is dependent on MTs, we quantitatively analyzed Rok distribution using a ubiquitously expressed GFP-tagged Rok transgene (Rok-GFP; Abreu-Blanco et al., 2014) in wild type and MT-disrupted SGs. Disruption of MTs by overexpression of spastin abolished the apicomedial accumulation of Rok in cells near the invagination pit, found in control SGs (Figs. 5A-B'' and G).

We also tested for accumulation of apicomedial Rok-GFP signals in *Dhc64C* RNAi and *klar* mutant SGs. Similar to spastin overexpression, reduction of *Dhc64C* levels led to more dispersed Rok signals along the apical domain of SG cells near the pit (Fig. 5C-C'' and G). In *klar* mutants, Rok-GFP tended to accumulate less profoundly and less uniformly in the apicomedial region of SG cells (Figs. 5E-E'') although not statistically significant compared to control (Fig. 5H). Overall, our data suggest that dynein-dependent intracellular trafficking along MTs regulates apical accumulation of Rok and apicomedial myosin formation during SG invagination.

Fog signaling activity is reduced when MTs are disrupted

Since Rok accumulation, apicomedial myosin formation, and subsequent coordinated apical constriction in the SG are Fog-dependent (Chung et al., 2017), we tested whether the roles of Fog signaling and MT trafficking in apical constriction were dependent on each other. Although the existing Fog antibody (Fuse et al., 2013) detected the endogenous Fog protein in the SG lumen at later stages, the signals at stage 11 were not strong enough to show precise subcellular localization of Fog in the SG. We therefore

overexpressed Fog in the SG to saturate the transport system and test a role of MTs in transporting Fog in this sensitized background. Consistent with our previous data that Fog signal mediates apicomedial Rok accumulation and apicomedial myosin formation (Chung et al., 2017), Fog-overexpressing SG cells over-accumulated Rok in the apicomedial region and dramatically increased apicomedial myosin (Figs. 6B,B'). This Fog gain-of-function effect on over-accumulation of Rok and increased apicomedial myosin was suppressed by spastin overexpression or *Dhc64C* knockdown (Figs. 6C-D', G-H',J,L). Interestingly, we also observed highly ruffled SG cell junctional morphology in almost all SG cells when Fog was overexpressed (Figs. 6I,I'). Similar cell distortions, albeit in a moderate level, have been observed during apical constriction in mesodermal cells (Martin et al., 2009) and in SG cells (Chung et al., 2017) when apicomedial myosin exerts the pulling force on adherens junctions. Indeed, increased apicomedial myosin was connected with E-Cad signals at distorted cell junctions (Figs. 6I,I'), suggesting that this ruffled junctional phenotype is due to increased pulling forces generated by high levels of apicomedial myosin upon increased Fog signaling activity. This convoluted junctional phenotype was suppressed by spastin overexpression or *Dhc64C* knockdown (Figs. 6G-H',K). Taken together, our data suggest that MTs and intracellular trafficking is necessary for Fog signaling activity and its downstream targets Rok and myosin, possibly by regulating transport of a key Fog signaling component(s) during SG invagination.

Disruption of MTs suppresses upregulation of the apical protein Crb

Transport of several key apical and junctional proteins is dependent on MTs and Rab11 (Jouette et al., 2019; Khanal et al., 2016; Le Droguen et al., 2015). One such protein is an apical transmembrane protein Crb, and Rab11 helps maintain apical Crb in the *Drosophila* ectoderm (Roeth et al., 2009). In the *Drosophila* SG and follicle cells, Crb is apically transported along MTs by the dynein motor (Myat and Andrew, 2002) (Aguilar-Aragon et al., 2019). Importantly, in *Drosophila* tracheae, loss of *crb* impairs apical constriction during the internalization process (Letizia et al., 2011).

272 Since Crb is upregulated near the invagination pit during SG invagination (Myat and
273 Andrew, 2002; Roper, 2012) (Figs. 7A,A'), we asked whether MT-dependent apical
274 transport of Crb is required for coordinated apical constriction in the SG. Using the same
275 genetic suppression strategy as we used for testing a role of MTs in Fog trafficking (Figs.
276 6C-C'), we co-overexpressed Crb and Spastin in the SG to test whether disruption of MTs
277 affects apical transport of Crb. A similar approach was taken in a recent study, where
278 overexpression of Crb provided a highly sensitive genetic background for identifying
279 components involved in Crb trafficking (Aguilar-Aragon et al., 2019). Consistent with
280 previous findings that Crb expression expands apical membranes in epithelial cells
281 (Chung and Andrew, 2014; Chung et al., 2017; Myat and Andrew, 2002; Wodarz et al.,
282 1993), overexpression of Crb resulted in enlarged apical areas of SG cells during
283 invagination (Figs. 7A-B'). Unlike control SG cells, Crb-overexpressing SG cells also
284 showed over-accumulation of Crb on the apical surface (Figs. 7B-B'). Co-overexpression
285 of Spastin and Crb suppressed this accumulation of Crb (Figs. 7C,C'), suggesting that
286 apical transport of Crb in the SG is dependent on MTs.

287

288 **Key apical and junctional proteins have a role in apical constriction during SG**
289 **invagination**

290 To test for a role of Crb in regulating apical constriction during SG invagination, we
291 knocked down *crb* in the SG using RNAi. Knockdown of *crb* resulted in reduction of Crb
292 levels compared to control (Sup. Figs. 2A-A''). Reduction of *crb* increased the number of
293 cells that have larger apical areas compared to control (Figs. 7D-E'). This data, along with
294 the dependence of apical transport of Crb on MTs (Figs. 7B-C'), suggest that normal Crb
295 levels in the apical domain are important in apical constriction during SG invagination.

296 We next tested whether knocking down key junctional proteins affects apical constriction
297 in the SG. Two such proteins, E-Cad and Baz/Par3, are trafficked by MTs in *Drosophila*
298 embryonic trachea (Le Droguen et al., 2015). During apical constriction, contractile forces
299 generated by the actomyosin complex are exerted on adherens junctions, with E-Cad
300 being a core component that integrates contractile forces to generate tension (Martin et

al., 2009). During amnioserosa apical constriction at *Drosophila* dorsal closure, Baz/Par3 in the Par complex regulates pulsed actomyosin contractions (David et al., 2010). Knockdown of *E-Cad* or *baz* in the SG led to reduced E-Cad or Baz levels at adherens junctions (Sup. Figs. 2B-C'') and resulted in defective apical constriction in the SG (Fig. 7F-G'). Quantification of the percentage of cells and cumulative percentage of cells of different apical areas showed a significant decrease in the number of constricting cells in *crb* and *baz* knockdown SGs (Fig. 7H). *E-Cad* knockdown SGs also displayed a similar trend although with less statistical significance (Fig. 7H). Overall, our data suggest a role of Crb, E-Cad and Baz in regulating apical constriction during SG invagination.

Reducing apical and junctional proteins affects Rok accumulation and apicomedial myosin formation

To test whether apical constriction defects observed in *crb*, *E-Cad* and *baz* knockdown SGs are linked to apicomedial myosin formation, we analyzed myosin levels in SGs with these knockdowns. Overall myosin levels were reduced in *crb* or *baz* knockdown SGs, both in the apicomedial region and at adherens junctions (Figs. 8A-A'',B-B'',D-D'',E). The ratio of apicomedial to junctional myosin was also reduced (Fig. 8E), suggesting that apical constriction defects in SGs depleted of *crb* or *baz* are, at least in part, due to failure of apicomedial myosin formation. In SGs depleted of *E-Cad*, myosin levels at each domain did not change significantly, but the ratio of apicomedial myosin to junctional myosin was significantly reduced compared to control (Fig. 8C-C'',E). Therefore, the apical constriction defects caused by *E-Cad* knockdown might be due to an imbalance of contractile forces.

Knockdown of *crb* or *baz* also resulted in Rok-GFP signals less accumulating in the apical region of cells near the invagination pit (Figs. 8G-I''). Quantification of the areas occupied by Rok-GFP puncta showed significant reduction in accumulation of apicomedial Rok when *crb* or *baz* was knocked down (Fig. 8J). Consistent with the relatively mild effect of *E-Cad* knockdown on apicomedial myosin (Figs. 8C-C'',E), Rok accumulation was not significantly affected by *E-Cad* knockdown. Several SG cells, however, showed dispersed

330 Rok-GFP signals in cells near the invagination pit, which was not observed in control cells
331 (Figs. 8 H-H'',J), suggesting some defects in Rok accumulation. Taken together, our
332 results suggest a role for Crb and Baz in regulating apical constriction by mediating Rok
333 accumulation and myosin activation during SG invagination.

334

335 **MTs play a role in trafficking apical and junctional proteins during SG formation**

336 To test a role of MTs in apical trafficking of Crb, E-Cad and Baz in the SG, we
337 overexpressed spastin throughout development and analyzed late stage SGs, where
338 apical trafficking is more easily detected in elongated SG cells. Analysis of spastin-
339 overexpressing SGs at stage 16 revealed that disruption of MTs resulted in short SG
340 tubes with a thin lumen compared to control SGs of the same stage (Figs. 9A,B).
341 Strikingly, whereas the majority of Rab11- and Nuf-positive vesicles localized in the apical
342 region of control SG cells (Figs. 9A-A'''), Rab11 and Nuf were observed as large
343 aggregates in the cytoplasm in spastin-overexpressing cells, overlapping with each other
344 (Figs. 9B-B'''). Our data suggest that MTs are required for apical enrichment of Rab11/Nuf
345 vesicles throughout SG tube formation.

346 Using the same co-overexpression strategy that we used for stage 11 (Figs. 7B-C'), we
347 tested whether MTs and Rab11 are required for apical trafficking of Crb also at stage 16.
348 Consistent with previous studies (Chung and Andrew, 2014; Wodarz et al., 1993), Crb
349 overexpression in the SG caused a dramatic increase of the apical membrane as well as
350 mislocalization of Crb basolaterally along the entire membrane (Figs. 9C-C''').
351 Overexpressing spastin along with Crb suppressed the apical membrane expansion
352 phenotype caused by Crb overexpression. Importantly, in these cells Crb mislocalized as
353 large cytoplasmic aggregates near the basolateral domain, which were largely
354 overlapping with mislocalized Rab11 (Figs. 9D-D'''). These data suggest that apical
355 transport of Crb in the SG is dependent on Rab11 and MTs.

356 We further tested a role for MTs in trafficking E-Cad and Baz in the SG, using the same
357 strategy as for Fog and Crb. Using UAS-Shotgun-GFP (Shg, *Drosophila* E-Cad) (Rørth,

358 2014) and UAS-Baz-GFP (Benton and St Johnston, 2003), we co-overexpressed E-Cad
359 or Baz with spastin in the SG. Overexpression of E-Cad-GFP alone did not result in overt
360 morphological defects in the SG, and punctate E-Cad signals mostly overlapped with Nuf
361 signals at and near adherens junctions (Figs. 9E-E'''). However, co-overexpression of E-
362 Cad-GFP and spastin resulted in aggregation of E-Cad in the basolateral region of SG
363 cells, which overlapped with Nuf (Figs. 9F-F'''). Similarly, overexpression of Baz-GFP in
364 the SG caused a slightly enlarged lumen (Figs. 9G-G'''). Baz-GFP signals were detected
365 mostly at adherens junctions, but small punctate structures were also detected in the
366 cytoplasm (Fig. 9G'). Overexpressing spastin along with Baz-GFP suppressed the
367 enlarged lumen phenotype caused by Baz overexpression (Figs. 9H-H'''). Importantly,
368 Baz-GFP signals observed as cytoplasmic punctate structures near the basolateral
369 domain that overlapped with Nuf-positive vesicles (Figs. 9H-H'''), suggesting that apical
370 transport of E-Cad and Baz in the SG is dependent on Rab11/Nuf and MTs. Overall, our
371 data suggest that several key proteins, including Crb, E-Cad and Baz, are trafficked
372 apically in a MT- and Rab11-dependent manner in the SG throughout tube formation.

373

374 **Discussion**

375 **MT-dependent intracellular trafficking during apical constriction**

376 Using the *Drosophila* SG, we demonstrate that MT-dependent intracellular trafficking is
377 critical for apical constriction during tissue invagination. MTs have been shown to have a
378 crucial role in stabilizing apical myosin during epithelial morphogenesis both in early
379 *Drosophila* embryos and in the *Drosophila* SG (Booth et al., 2014; Ko et al., 2019).
380 Particularly in the SG, MTs interact with apicomedial myosin via Short stop, the
381 *Drosophila* spectraplakin, emphasizing a direct interplay between the MT and the apical
382 myosin networks (Booth et al., 2014). Our data reveals another role of MTs in regulating
383 protein trafficking to control the apical myosin networks during tissue invagination. During
384 SG invagination, a network of longitudinal MT bundles is observed near the invagination
385 pit (Booth et al., 2014). Our data shows apical enrichment of key endocytic markers in the
386 same area and that this enrichment is important for forming the apicomedial myosin

387 networks (Figs. 1-4), suggesting a link between localized protein trafficking along MTs to
388 apical myosin regulation. Our data support a model that dynein- and Rab11-dependent
389 intracellular trafficking is crucial for organizing apical myosin networks during apical
390 constriction in the SG.

391 Interestingly, cytoplasmic dynein is associated with cellular structures and exerts tension
392 on MTs. For example, dynein tethered at the cell cortex can apply a pulling force on the
393 MT network by walking towards the minus end of a MT (Laan et al., 2012). In interphase
394 cells, force generated by dynein also regulates MT turnover and organization (Yvon et
395 al., 2001). Therefore, we do not rule out the possibility that reduced dynein functions could
396 affect MT organization and/or a pulling force on the MT networks regardless of its role in
397 intracellular trafficking, which will subsequently affect apical myosin structures during SG
398 invagination. However, we favor the apical trafficking model as we did not observe overt
399 changes in the MT networks in *Dhc64C* RNAi SGs (data not shown).

400

401 **Integrating apical and junctional proteins with actomyosin networks during SG**
402 **invagination**

403 During branching morphogenesis in *Drosophila* trachea, MTs and dynein motors have a
404 critical role in proper localization of junctional proteins such as E-Cad and Baz (Le
405 Droguen et al., 2015). This is consistent with our observations with MT-dependent
406 trafficking of Crb, E-Cad and Baz in the late stage SG (Fig. 9), suggesting a conserved
407 role of MT-dependent intracellular trafficking in junctional remodeling and stabilization
408 during epithelial tube formation. Our data suggests that proper levels of apical and
409 junctional proteins are also important for tissue invagination at the beginning of epithelial
410 tube formation. Dispersed Rok and less prominent apicomedial myosin are observed in
411 invaginating SGs upon knockdown of *crb*, *E-Cad* and *baz* (Fig. 8), suggest a requirement
412 of apical and junctional proteins in proper organization of apical actomyosin networks
413 during epithelial tube formation. We propose that MTs and Rab11 play a role in apical
414 trafficking of these proteins during SG invagination and throughout SG tube formation.

415 When *crb* is knocked down using RNAi in the SG, overall intensity of myosin is decreased
416 near the invagination pit, for both apicomedial and junctional pools (Fig. 8). It is possible
417 that proper Crb levels are required for modulating myosin activity both in the apical
418 domain and at junctions, which contribute to apical constriction and cell rearrangement
419 during SG invagination. Anisotropic localization of Crb and myosin was observed at the
420 boundary of the SG placode, where myosin accumulates at edges where Crb is lowest
421 (Roper, 2012). Planar polarization of Rok at this boundary is modulated through
422 phosphorylation by Pak1 downstream of Crb (Sidor et al., 2020). It will be interesting to
423 further test how Crb might affect junctional myosin dynamics and SG invagination.

424 As contractile actomyosin structures exert forces on adherens junction to drive apical
425 constriction, we speculate that slight reduction of apicomedial myosin upon *E-Cad* RNAi
426 might be due to reduction of cell adhesion. Also, decrease of apicomedial and junctional
427 myosin caused by *baz* knockdown is consistent with the role of the Par complex in
428 regulating pulsed actomyosin contraction during *Drosophila* dorsal closure (David et al.,
429 2010). It will be interesting to determine if coordination of apical and junctional proteins
430 and apical cytoskeletal networks through intracellular trafficking is conserved during
431 tubular organ formation in general.

432

433 **Regulation of Fog signaling activity**

434 The Fog pathway represents one of the best-understood signaling cascades controlling
435 epithelial morphogenesis (Manning and Rogers, 2014). Although best studied in
436 *Drosophila*, the pathway components have been also identified in other insects,
437 suggesting a more widely conserved role of Fog signaling in development (Benton et al.,
438 2019; Urbansky et al., 2016). The dorsal/posterior region of the SG where Dhc64C is
439 apically enriched (Fig. 1) correlates with localized Fog signaling activity that promotes
440 clustered apical constriction (Chung et al., 2017). Disruption of MTs or *Dhc64C*
441 knockdown not only causes dispersed Rok and defective apicomedial myosin (Fig. 5),
442 which is reminiscent of *fog* mutant phenotypes, but also suppresses the Fog gain-of-
443 function effect on Rok and myosin (Fig. 6). We propose that dynein-dependent apical

444 trafficking is important for regulating Fog signaling activity to control apical constriction
445 during epithelial tube formation, with the Fog ligand and/or the as yet unidentified SG
446 receptor(s) of Fog being possible cargos of dynein.

447 Apical enrichment of Rab11/Nuf is also MT-dependent during SG invagination and
448 disruption of the Rab11 function inhibits apical constriction in SGs (Fig. 3). Unlike other
449 apical or junctional proteins that we have tested (Crb, E-Cad and Baz) that colocalize with
450 Rab11/Nuf when mislocalized, mislocalized Fog did not co-localize with Rab11 or Nuf
451 (Sup. Fig. 3). It could be explained by the fact that Rab11 is primarily associated with
452 recycling endosomes; when Fog is not used, it is most likely degraded rather than
453 recycled. As recycling of membrane receptors to the cell surface plays an important role
454 in the regulation of overall signaling activity, it is possible that Rab11 is also involved in
455 recycling of the Fog receptor(s) to regulate Fog activity in the SG. Indeed, several GPCRs
456 are recycled via Rab11 (Anborgh et al., 2000; Cerniello et al., 2017; Dale et al., 2004; Fan
457 et al., 2003; Hamelin et al., 2005; Hunyady et al., 2002; Innamorati et al., 2001; Volpicelli
458 et al., 2002). Further work needs to be done to fully understand the mechanisms
459 underlying trafficking of Fog and its receptor(s) and how the signaling pathway is able to
460 generate cellular forces to drive cell shape changes during epithelial morphogenesis.

461

462 **Materials and Methods**

463 **Fly stocks and husbandry**

464 Fly lines used in our experiments were listed in a separate table. All crosses were
465 performed at 25°C, unless stated otherwise.

466

467 **Antibody staining and confocal microscopy**

468 Antibodies used in our experiments were listed in a separate table. Embryos were
469 collected on grape juice-agar plates and processed for immunofluorescence using
470 standard procedures. Briefly, embryos were dechorionated in 50% bleach, fixed in 1:1

471 heptane:formaldehyde for 40 min and devitellinized with 80% EtOH, then stained with
472 primary and secondary antibodies in PBSTB (1X PBS, 0.1% Triton X-100, 0.2% BSA).
473 For acetylated α-tubulin, tyrosinated α-tubulin staining, embryos were hand-devitellinized.
474 All images were taken with a Leica SP8 confocal microscope.

475

476 **Cell segmentation and apical area quantification**

477 Embryos immunostained with E-Cad and CrebA were imaged using a Leica SP8 confocal
478 microscope. Since Rok accumulation, apicomedial myosin and apical constriction depend
479 on the depth of invagination in the SG, SGs that were invaginated within the range of 5.1-
480 9.9 μm depth were used for quantification for proper comparison between different
481 genotypes. Maximum intensity projection was generated from three apical focal planes
482 with highest E-Cad signals for all genotypes, except for maternal/zygotic knockdown of
483 *Dhc64C*, where 10 to 30 focal planes were used due to wavy epithelial morphology (0.3
484 μm apart for each focal plane). Cells were segmented along the E-Cad signals and cell
485 areas were calculated using the Imaris Program (Bitplane). Since the Imaris Program
486 calculated the areas of both the front and the back of the projected cell layer, we divided
487 the measured areas by two to get the true values of apical areas of SG cells.

488

489 **Negative correlation between apical area and Rab11/Nuf intensity**

490 Cell segmentation for five WT SGs within the range of 5.1- 9.9 μm invagination was
491 performed as described above. Intensity mean was measured for the entire Rab11/Nuf
492 signals for each segmented cell using the Imaris Program (Bitplane) and plotted.
493 Correlation (Pearson) and P values were calculated using the GraphPad Prism software.

494 To compare the enrichment of Rab11/Nuf near the invagination pit of the WT SG to the
495 Spastin overexpressed SG, the ratio of deviation of Rab11/Nuf intensity to median
496 Rab11/Nuf intensity was used. Median value of Rab11/Nuf intensity is the average of
497 Rab11/Nuf mean intensities in all SG cells. Deviation of Rab11/Nuf intensity is the

498 difference between the mean intensity of each cell and the median value. Five WT SGs
499 (690 cells) and four Spastin-overexpressed SGs (396 cells) were analyzed and plotted.
500 P values were calculated using the Mann-Whitney U test in the GraphPad Prism software.

501

502 **Colocalization analysis**

503 Colocalization analyses were performed with the JACOP plugin in Fiji software.
504 Thresholded Manders' overlap coefficients were used to show the extent to which two
505 proteins colocalize. Manders' coefficients, vary from 0 to 1, are indicators of overlap
506 between two proteins and are independent of signal proportionality. The Manders' overlap
507 coefficient for Rab11 is the proportional Rab11 that is colocalized with tyrosinated α-
508 tubulin. The Manders' overlap coefficient for tyrosinated α-tubulin is the proportional
509 tyrosinated α-tubulin that is colocalized with Rab11. For each SG, the dorsal/posterior
510 region of 100 μm^2 where Rab11 is upregulated was tested. Six WT embryos were used
511 for quantification.

512

513 **Quantification of the intensity of myosin, Crb, E-Cad and Baz**

514 For all myosin quantification, maximum intensity projections that span the apical and the
515 junctional region of SG cells were used (Leica LasX) and measurements were performed
516 using the Fiji software. A group of 10 cells in the dorsal/posterior region of SG placode
517 near the invagination pit were selected for quantification. Regions were drawn manually
518 along the inner or outer boundary of E-Cad signals of each cell to calculate the mean
519 intensity of apicomedial and junctional myosin. For background correction, mean intensity
520 of apicomedial myosin in ten cells outside of the SG placode was measured. The average
521 value of mean intensities of apicomedial myosin in these ten cells was used to subtract
522 the background of the cells inside the placode from the same embryo. For each genotype,
523 five SGs were used for quantification. P values were calculated using the Mann-Whitney
524 U test in the GraphPad Prism software. Mean intensities of Crb, E-Cad and Baz were

525 measured with the same method used for quantifying the mean intensity of junctional
526 myosin.

527

528 **Quantification of area of Rok puncta**

529 A single confocal section that had the strongest medial Rok signals was selected. Cell
530 boundaries were labeled by immunostaining with the antibody against E-Cad. To analyze
531 Rok distribution, we performed particles analysis using the Fiji software. 15 cells in the
532 dorsal/posterior region near the invagination pit were selected for quantification. Rok-GFP
533 signals were converted into black-and-white using the *Threshold* tool in Photoshop before
534 analysis. Using the *Analyze particles* tool in Fiji, Rok-GFP puncta with areas equal or
535 larger than 0.02 μm^2 were measured. Five SGs were used for quantification. P values
536 were calculated using the Mann-Whitney U test in the GraphPad Prism software.

537

538 **Quantification of tortuosity**

539 10 cells in the dorsal/posterior region near the invagination pit of the SG placode were
540 selected for quantification. Using the Fiji software, the actual length of a given adherens
541 junction (L) was calculated using the E-Cad signals. The tortuosity was calculated as the
542 ratio of the junctional length (L) and the shortest distance (L_o) between the two vertices
543 (tortuosity= L/L_o). Five SGs were used for quantification for each genotype. P values were
544 calculated using the Mann-Whitney U test in the GraphPad Prism software.
545

Fly strains	**Source**	**RRID**	**References**
UAS-Spastin (on II)	N. Sherwood, Duke		Sherwood et al., 2004
UAS-Spastin-CFP (on III)	N. Sherwood, Duke		Du et al., 2010
fkh-Gal4 (on II)	D. Andrew (John Hopkins University)		Chung et al., 2017
fkh-Gal4 (on III)	D. Andrew (John Hopkins University)		Chung et al., 2017
ubi-Rok-GFP	S. Parkhurst (Fred Hutchinson Cancer Research Center)		Abreu-Blanco et al., 2014
sqh-GFP			Royou et al., 2004
UAS-Rab11S25N-EYFP	Bloomington Stock Center	9792, 23261	
UAS-Dicer-2	Bloomington Stock Center	60008	
UAS-Dhc64C RNAi	Bloomington Stock Center	76941, 28749, v28053, v28054.	

	Vienna *Drosophila* Resource Center	4 lines worked equally. v28054 was used for all of the data shown in this work.	
klar^{1}	Bloomington Stock Center	3256	
klar^{mCD4}	Bloomington Stock Center	25097	
klar^{mCD4} *ubi-Rok-GFP*	Recombinant line generated from *klar*^{mCD4} and *ubi-Rok-GFP*		
UAS-Crb RNAi	Bloomington Stock Center	38373, 38903, 40869, 34999. 4 lines worked equally. 2 lines (38373, 34999) were used for the data shown in this work.	
UAS-Baz RNAi	Bloomington Stock Center	35002, 38213, 39072.	

		38213 provided the strongest phenotype and used for quantification in this work.	
UAS-E-Cad RNAi	Bloomington Stock Center	32904	
UAS-Shg-GFP	Bloomington Stock Center	58445	
UAS-Baz-GFP	Bloomington Stock Center	65845	
matα4-Gal4 (*maternal Gal4*; on II)	Bloomington Stock Center	7062	

546

547

548

Antibody	Source	RRID	Dilution
α-E-Cad (rat)	DSHB (deposited by T. Uemura, Kyoto University)	DCAD2 (AB_528120)	1:50
α-CrebA (rat)	Andrew lab (John Hopkins University)		1:3000
α-CrebA (rabbit)	Andrew lab (John Hopkins University)		1:5000
α-Dhc (mouse)	DSHB (deposited by J.M. Scholey, University of California)	2C11-2 (AB_2091523)	1:50
α-Rab11 (rabbit)	Andrew lab (John Hopkins University)		1:500
α-Nuf (guinea pig)	Sotillos lab (CABD)		1:500
α-acetylated α-tubulin (mouse)	Invitrogen	32-2700 (AB_2533073)	1:1000
α-tyrosinated α-tubulin (rat)	Invitrogen	MA1-80017 (AB_2210201)	1:1000
α-GFP (chick)	Invitrogen	A10262 (AB_2534023)	1:500

α-β-galactosidase (rabbit)	Invitrogen	A11132 (AB_221539)	1:500
α-Crb (mouse)	DSHB (deposited by E. Knust, Max Planck Institute)	Cq4 (AB_528181)	1:10
α-Fog (rabbit)	N. Fuse (Fuse et al., 2013)		1:1000
α-Sec15 (guinea pig)	Bellen lab (Baylor College of Medicine)		1:2000
Alexa Fluor 488/568/647-coupled secondary antibodies	Invitrogen		1:500

549

550

Acknowledgments

We thank the members of the Chung laboratory for comments and suggestions. We thank A. Martin, S. Parkhurst and N. Sherwood and the Bloomington stock center for fly stocks, and D. Andrew, H. Bellen, S. Sotillos and the Developmental Studies Hybridoma Bank for antibodies. We thank Flybase for the gene information. We are grateful to A. Bohnert, C. Hanlon, A. Johnson and C. O'Kane for their helpful comments on the manuscript. This work is supported by start-up fund from Louisiana State University and the grant from the Board of Regents Research Competitiveness Subprogram GR-00005224 to S.C.

561 **Figure legends**

562 **Fig. 1. Intracellular trafficking components are apically enriched near the**
563 **invagination pit.** (A) A schematic drawing of the anterior region of the *Drosophila* embryo
564 for stage 11 (ventral and lateral views) and stage 16 (lateral view). Green, SGs. Top right,
565 magnified view of a SG placode. Purple area, the region where SG cells undergo
566 clustered apical constriction during invagination. (B-D) A wild type SG immunostained for
567 E-Cad, Rab11 and Nuf. Rab11 and Nuf show upregulation near the invagination pit. Red
568 arrowheads, Rab11 and Nuf signals near the segmental groove. (B'-D') Heat maps of
569 apical area (B') and intensity of Rab11 and Nuf (C', D'). Cells with small apical areas (dark
570 blue cells in B') near the invagination pit show high intensity of Rab11 and Nuf (red cells
571 in C' and D'). (E) Negative correlation between Rab11/Nuf intensities and apical areas of
572 SG cells. R, Pearson correlation coefficient. $p<0.0001$ for all samples (n=5 SGs; 690
573 cells). (F-H') Rab11-EYFP SG labeled with E-Cad (F), GFP (G) and Nuf (H) and
574 corresponding heat maps for apical areas (F') and intensity of GFP (G') and Nuf signals
575 (H'). Rab11-EYFP shows the same enrichment near the invagination pit. (F'-H') (I-J') A
576 wild type SG immunostained with E-Cad (I) and Dhc64C (J) and corresponding heat maps
577 for apical areas (I') and intensity of Dhc64C signals (J'). (K-L') A Rab7-EYFP SG
578 immunostained with E-Cad (K) and GFP (L) and corresponding heat maps for apical
579 areas (K') and intensity of Rab7-EYFP (L'). Asterisks: invagination pit. White lines: SG
580 boundary.

Figure 1

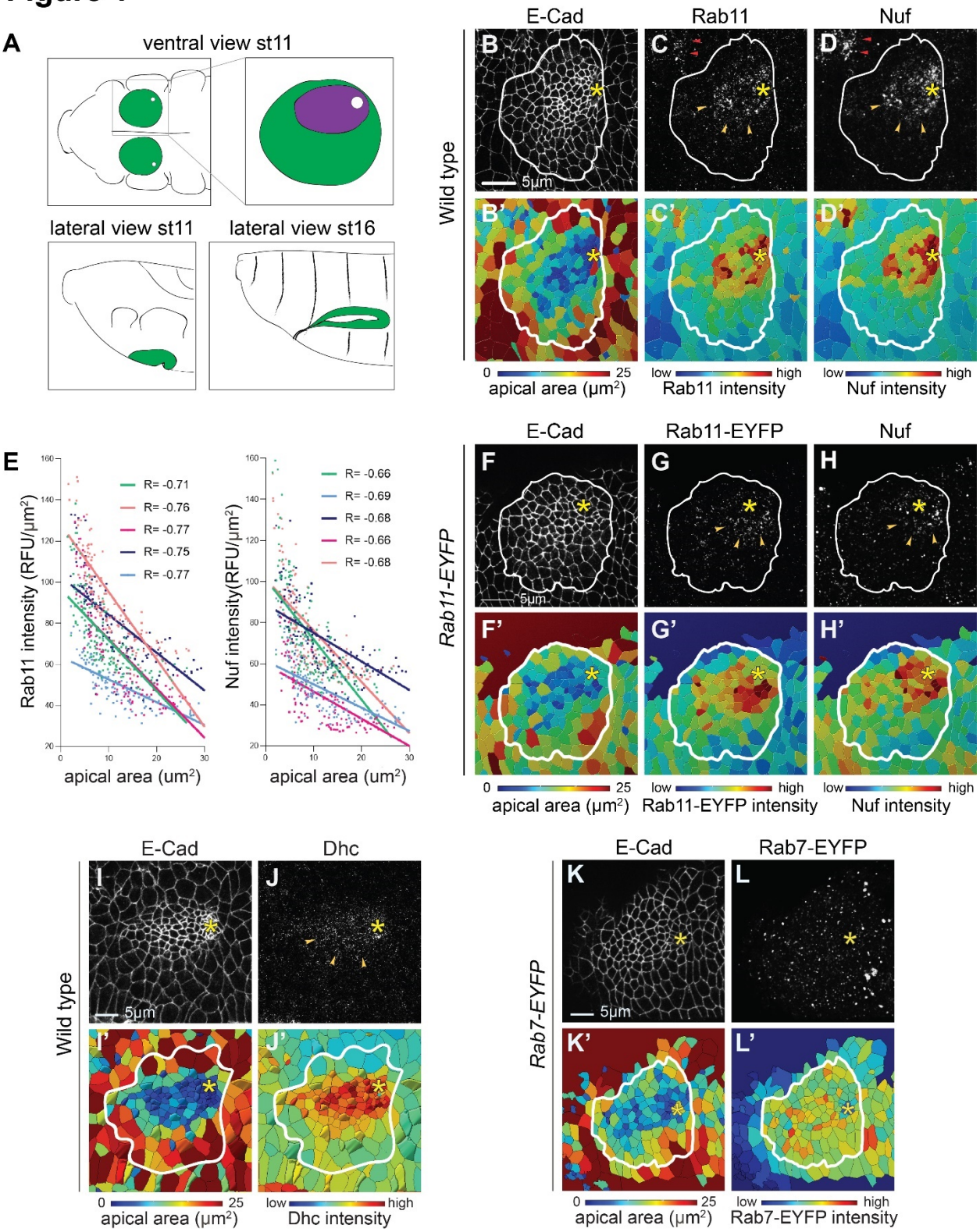
A
ventral view st11
lateral view st11
lateral view st16
E-Cad
Rab11
Nuf
Wild type
B
C
D
B'
C'
D'
5µm
0
25
apical area (µm²)
low
high
Rab11 intensity
Nuf intensity
E
Rab11 intensity (RFU/µm²)
Nuf intensity(RFU/µm²)
apical area (um²)
R= -0.71
R= -0.76
R= -0.77
R= -0.75
R= -0.77
R= -0.66
R= -0.69
R= -0.68
R= -0.66
R= -0.68
Rab11-EYFP
F
G
H
F'
G'
H'
Rab11-EYFP intensity
E-Cad
Dhc
I
J
I'
J'
Dhc intensity
E-Cad
Rab7-EYFP
K
L
K'
L'
Rab7-EYFP intensity

584 **Fig. 2. Disruption of MTs results in uncoordinated apical constriction, reduction of**
585 **apical vesicle numbers, and mislocalization of Rab11/Nuf.**

586 (A-A’’’) Co-localization of Rab11 and tyrosinated α-tubulin in SG cells during invagination.
587 A wild type SG immunostained with Rab11 (green) and tyrosinated α-tubulin (purple; Tyr-
588 α-Tub) is shown with higher magnification of the yellow boxed area (A’-A’’’). Yellow
589 arrowheads, co-localized Rab11 and tyrosinated α-tubulin. (B-B’’) Z sections along the
590 yellow line in (A). Yellow arrowheads, co-localized Rab11 and tyrosinated α-tubulin. (C)
591 Thresholded Manders’ colocalization coefficients show the extent to which two proteins
592 colocalize (n= 6 SGs). (D-E’’’) Overexpression of spastin in the SG disrupts the MT
593 networks and compromises enrichment of Rab11 near the invagination pit. (D-D’’’) En
594 face (top) and lateral (bottom) views of a control SG show abundant levels of tyrosinated
595 α-tubulin (D’’) and acetylated α-tubulin (D’’’; Ace-α-Tub). Rab11 is enriched in the apical
596 domain near the invagination pit (yellow arrowheads). (E-E’’’) Overexpression of spastin
597 by *fkh-Gal4* leads to a loss of MTs in the SG, labelled both by tyrosinated α-tubulin (E’’)
598 and acetylated α-tubulin (E’’’). (E’) Rab11 is not enriched near the invagination pit and
599 mislocalizes basolaterally when spastin is overexpressed (red arrowheads). (F-F’’)
600 Confocal images of a spastin-overexpressing SG stained with Rab11 (F’) and Nuf (F’’)
601 and corresponding heat maps for apical areas (G), intensities of Rab11 (G’) and Nuf (G’’).
602 Compare to control SGs in Figs. 1B-H’. (H) A ratio of deviation of intensity to the median
603 intensity of Rab11 (left) and Nuf (right) in all SG cells (n= 5 SGs; 690 cells). *, $p<0.01$.
604 ****, $p<0.0001$, Mann-Whitney U test. Asterisks: invagination pit. White lines: SG
605 boundary.

Figure 2

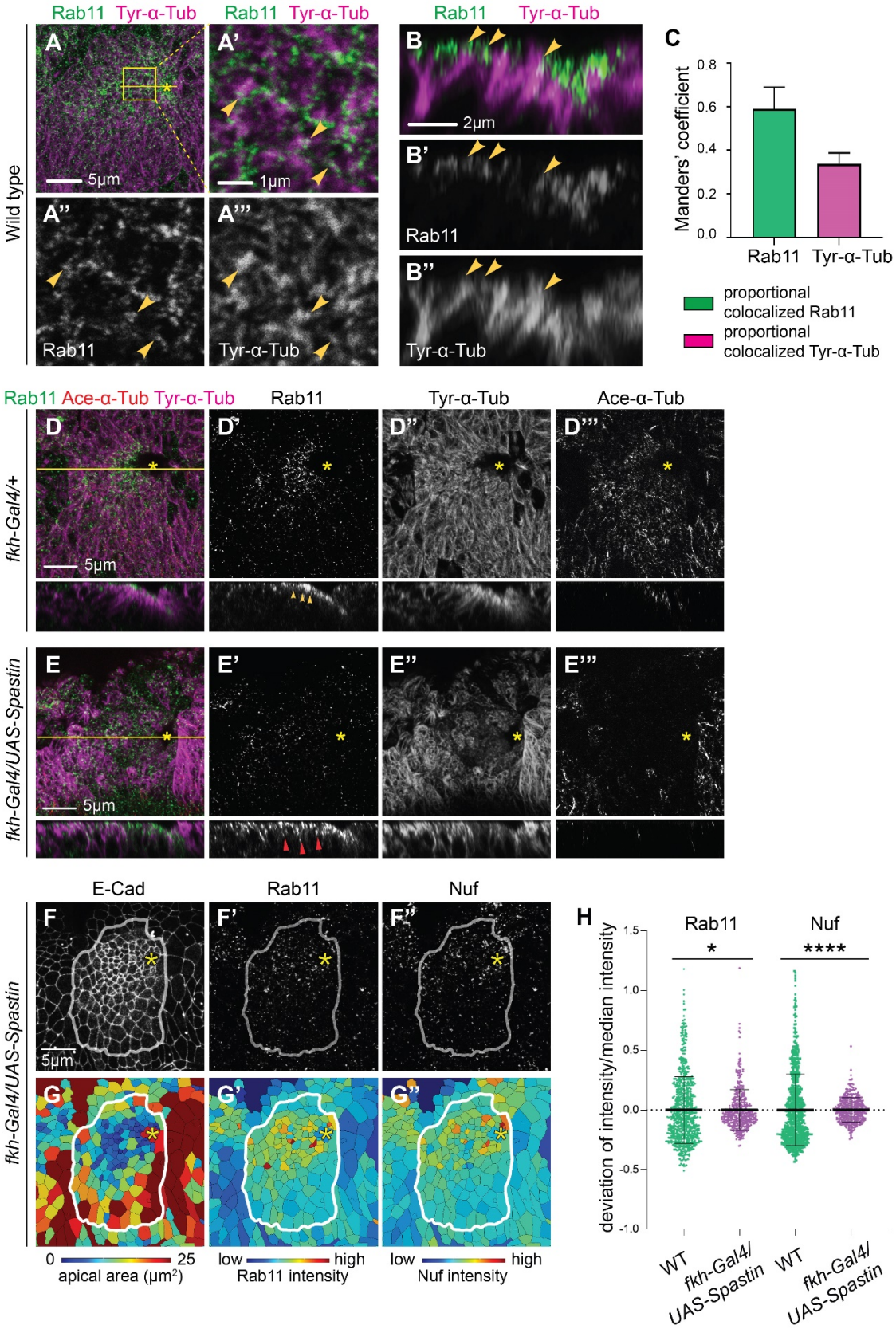
Rab11 Tyr-α-Tub
Rab11 Tyr-α-Tub
Rab11 Tyr-α-Tub
Wild type
A
A'
B
B'
B''
A''
A'''
5μm
1μm
2μm
Rab11
Tyr-α-Tub
C
Manders' coefficient
0.8
0.6
0.4
0.2
0.0
Rab11 Tyr-α-Tub
proportional colocalized Rab11
proportional colocalized Tyr-α-Tub
Rab11 Ace-α-Tub Tyr-α-Tub
Rab11
Tyr-α-Tub
Ace-α-Tub
fkh-Gal4/+
D
D'
D''
D'''
fkh-Gal4/UAS-Spastin
E
E'
E''
E'''
E-Cad
Rab11
Nuf
F
F'
F''
G
G'
G''
0 25
apical area (μm²)
low high
Rab11 intensity
low high
Nuf intensity
H
Rab11
Nuf
*
****
deviation of intensity/median intensity
1.5
1.0
0.5
0.0
-0.5
-1.0
WT
fkh-Gal4/ UAS-Spastin
WT
fkh-Gal4/ UAS-Spastin

606

607 **Fig. 3. Rab11 and the dynein motor are required for coordinated apical constriction**
608 **in the SG.**

609 (A-C) Confocal images of control (A), Rab11-DN-overexpressing (B) and *Dhc64C* RNAi
610 (C) SGs stained with E-Cad. (A'-C') Heat maps corresponding to images shown in A-C.
611 (D-E') Confocal images and corresponding heat maps of wild type (D, D') and *klar* mutant
612 (E, E') SGs. (F, H) Percentage and cumulative percentage of cells with different apical
613 areas. Mann-Whitney U test (for percentage of cells) and Kolmogorov-Smirnov test (for
614 cumulative percentage of cells). n= 5 SGs (control (*fkh-Gal4/*+), 517 cells; *Rab11-DN*,
615 536 cells; zygotic *Dhc* RNAi, 499 cells; WT, 690 cells; $klar^1$, 705 cells; maternal/zygotic
616 *Dhc* RNAi, 561 cells). **, $p<0.01$; ****, $p<0.0001$. (G) A range of phenotypes is observed
617 when *Dhc64C* is knocked down both maternally and zygotically, including mild
618 (uncoordinated apical constriction), intermediate (enlarged pit) and severe (deformed
619 epithelial tissue and additional folds) phenotypes. Asterisks: invagination pit. White lines:
620 SG boundary.

621

Figure 3

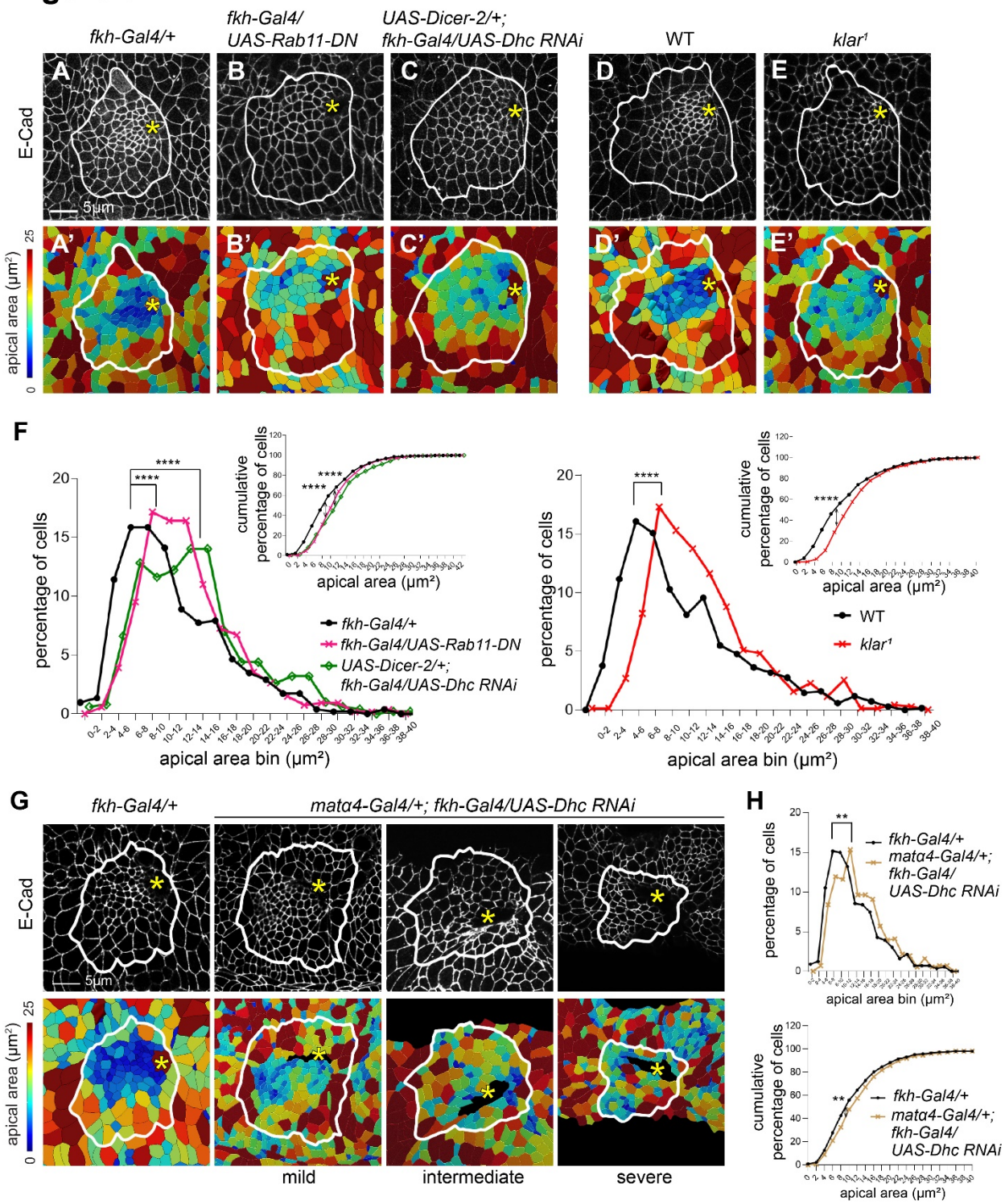

622

623

624

625 **Fig. 4. Compromised intracellular trafficking leads to a reduction of apicomedial**
626 **myosin formation in the SG cells.**

627 (A-B’’’’) sqh-GFP signals in control (A-A’’’’) and *Dhc64C* RNAi (B-B’’’’) SGs. (A’’-B’’’’)
628 Higher magnification of the yellow boxed area in A and B. *Dhc64C* knockdown leads to
629 reduced apicomedial myosin (red arrowheads in B’’). Compare to strong signals of
630 apicomedial myosin in A’’ (yellow arrowheads). (C) Quantification of apicomedial myosin,
631 junctional myosin and the ratio of apicomedial to junctional myosin in *Dhc64C* RNAi SG
632 cells. (D-E’’’’) Myosin signals in control (D-D’’’’) and in *klar* mutant (E-E’’’’) SGs. (D’’-E’’’’)
633 Higher magnification of the yellow boxed area in D and E. *Dhc64C* knockdown leads to
634 reduced apicomedial myosin (red arrowheads in E’’); compare these to strong signals of
635 apicomedial myosin in D’’ (yellow arrowheads). (F) Quantification of apicomedial myosin,
636 junctional myosin and the ratio of apicomedial to junctional myosin in control and *klar*
637 mutant SG cells. n= 5 SGs for all genotypes; 10 cells in the dorsal/posterior region of
638 each SG. *, $p< 0.05$. **, $p< 0.01$. ***, $p< 0.001$. ****, $p<0.0001$, Mann-Whitney U test.
639 Asterisks: invagination pit.

Figure 4

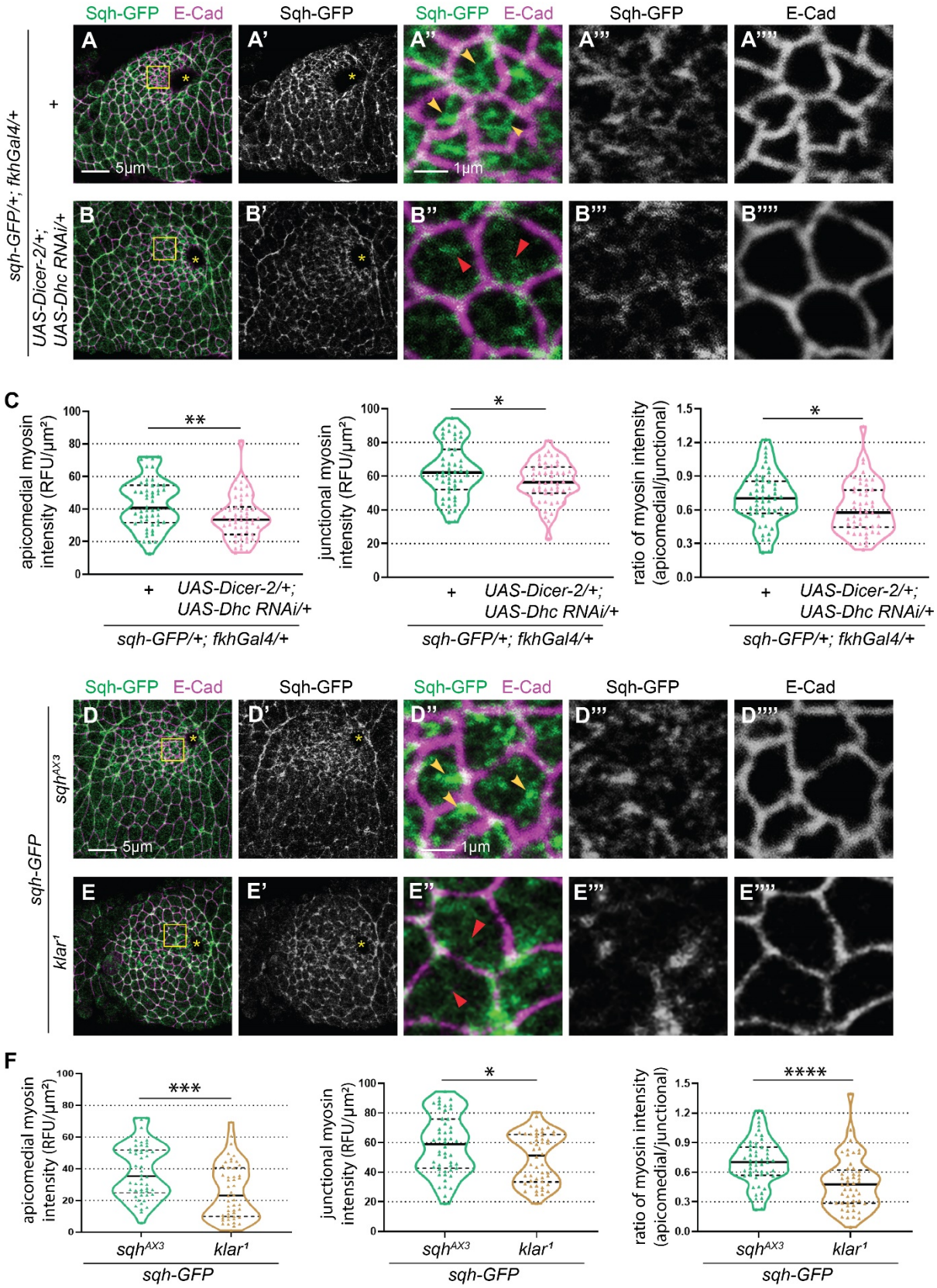
Sqh-GFP E-Cad
Sqh-GFP
Sqh-GFP E-Cad
Sqh-GFP
E-Cad
A
A'
A''
A'''
A''''
B
B'
B''
B'''
B''''
5µm
1µm
sqh-GFP/+; fkhGal4/+
+
UAS-Dicer-2/+; UAS-Dhc RNAi/+
C
apicomedial myosin intensity (RFU/µm²)
junctional myosin intensity (RFU/µm²)
ratio of myosin intensity (apicomedial/junctional)
**
*
*
D
D'
D''
D'''
D''''
E
E'
E''
E'''
E''''
sqh-GFP
sqhAX3
klar1
F
apicomedial myosin intensity (RFU/µm²)
junctional myosin intensity (RFU/µm²)
ratio of myosin intensity (apicomedial/junctional)
***
*
****

640

641 **Fig. 5. Compromised MT-based intracellular trafficking impairs accumulation of**
642 **apicomedial Rok within constricting cells during invagination.** (A-A'') A control SG
643 shows accumulation of Rok-GFP signals (green) in the apicomedial region of cells near
644 the invagination pit. E-Cad (magenta), cell boundary. Yellow arrowheads, accumulative
645 Rok-GFP. (B-C'') Rok-GFP signals are more dispersed in SG cells upon spastin
646 overexpression (B-B'') and knockdown of *Dhc64C* (C-C'') (red arrowheads). (D) A control
647 SG homozygous for ubi-Rok-GFP shows a huge accumulation of Rok-GFP in constricting
648 cells (yellow arrowheads). (E) A mutation in *klar* results in slightly reduced accumulation
649 of Rok-GFP in cells near the invagination pit (red arrowheads). (F) Representative images
650 for how areas of Rok-GFP puncta were measured using the Fiji software. (G, H)
651 Quantification of areas of Rok-GFP puncta. ****, $p < 0.0001$, Mann-Whitney U test. n= 5
652 SGs for all genotypes; 15 cells in the dorsal/posterior region for each SG.
653

Figure 5

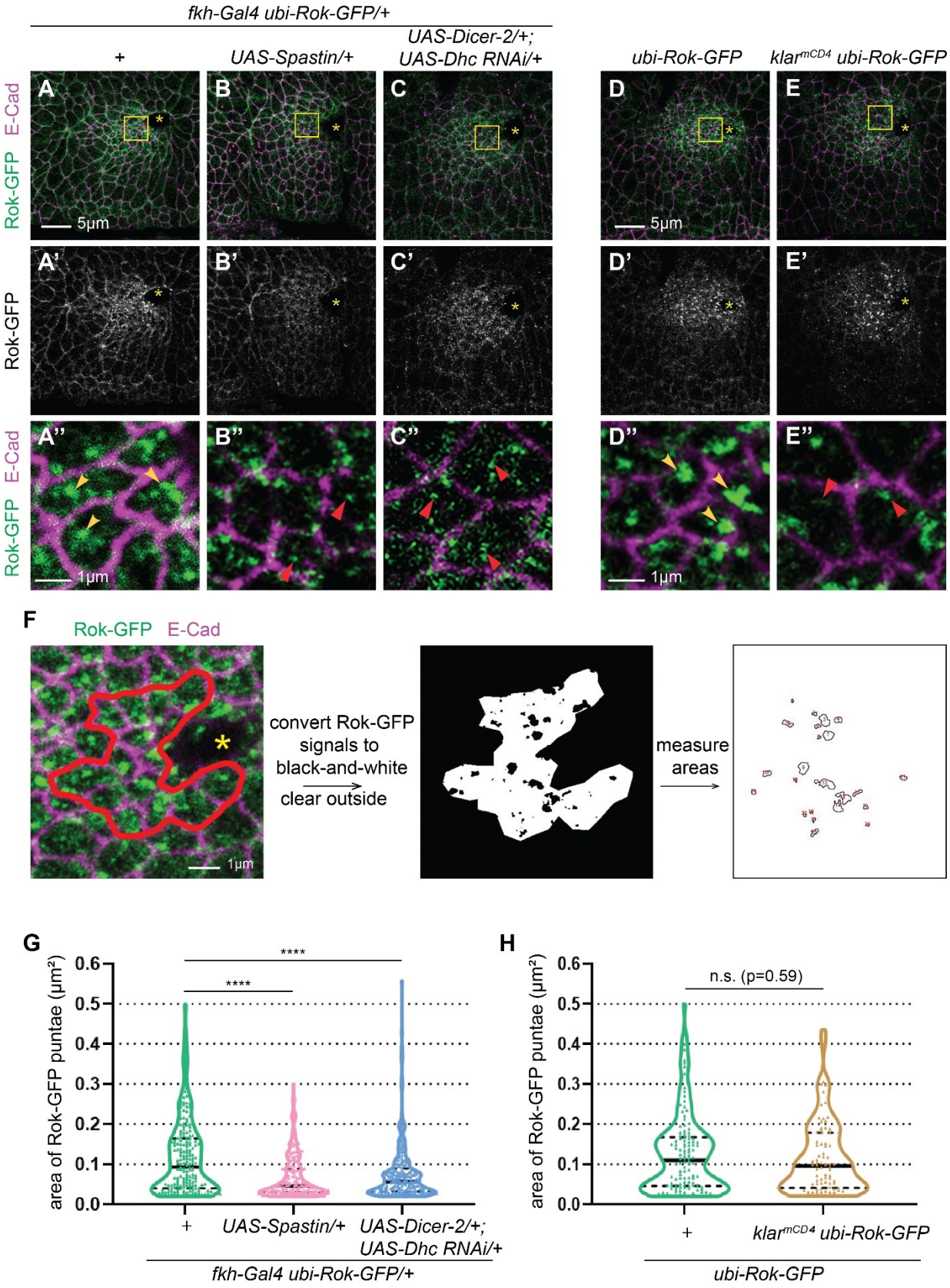
fkh-Gal4 ubi-Rok-GFP/+
+
UAS-Spastin/+
UAS-Dicer-2/+; UAS-Dhc RNAi/+
ubi-Rok-GFP
klarmCD4 ubi-Rok-GFP
Rok-GFP E-Cad
Rok-GFP
Rok-GFP E-Cad
A
B
C
D
E
A'
B'
C'
D'
E'
A''
B''
C''
D''
E''
5µm
1µm
F
Rok-GFP E-Cad
convert Rok-GFP signals to black-and-white
clear outside
measure areas
G
area of Rok-GFP puntae (µm²)
0.0
0.1
0.2
0.3
0.4
0.5
0.6
****
****
+
UAS-Spastin/+
UAS-Dicer-2/+; UAS-Dhc RNAi/+
fkh-Gal4 ubi-Rok-GFP/+
H
n.s. (p=0.59)
klarmCD4 ubi-Rok-GFP
ubi-Rok-GFP

654

655 **Fig. 6. Impairing microtubule-based trafficking suppresses the over-active Fog**
656 **signaling pathway.** (A-A') Rok-GFP signals in constricting cells in a control SG (yellow
657 arrowheads). (B-B') In Fog-overexpressing SGs, Rok-GFP is over-accumulated in cells
658 (red arrowheads). (C-D') The Rok over-accumulation phenotype is suppressed when
659 spastin is overexpressed or *Dhc64C* is knocked down (red arrows). (E-E') Apicomedial
660 myosin in the control SG (yellow arrowheads). (F-F') Fog-overexpressing SG cells show
661 increased apicomedial myosin (red arrowheads). (G-H') Upregulation of apicomedial
662 myosin caused by Fog overexpression is inhibited when spastin is overexpressed or
663 *Dhc64C* is knocked down (red arrows). (I-I') Fog overexpressing SG cells show wavy
664 adherens junctions (E-Cad) signals. Cell junctions are deformed at the contact sites to
665 apicomedial myosin (red arrowheads). (J) Quantification of areas of Rok-GFP puncta. (n=
666 5 SGs; 15 cells for each SG). (K) Left, a cartoon for how the tortuosity of a cell junction
667 was measured. Right, quantification of the tortuosity (n= 5 SGs; 10 cells for each SG;
668 ~280 junctions). (L) Quantification of apicomedial myosin, junctional myosin and the ratio
669 of apicomedial myosin to junctional myosin (n= 5 SGs; 10 cells for each SG). For all
670 quantification, cells in the dorsal/posterior region of SG placode were used. *, $p< 0.05$. **,
671 $p< 0.01$. ***, $p< 0.001$. ****, $p< 0.0001$, Mann-Whitney U test. Asterisks: invagination pit.

672

Figure 6

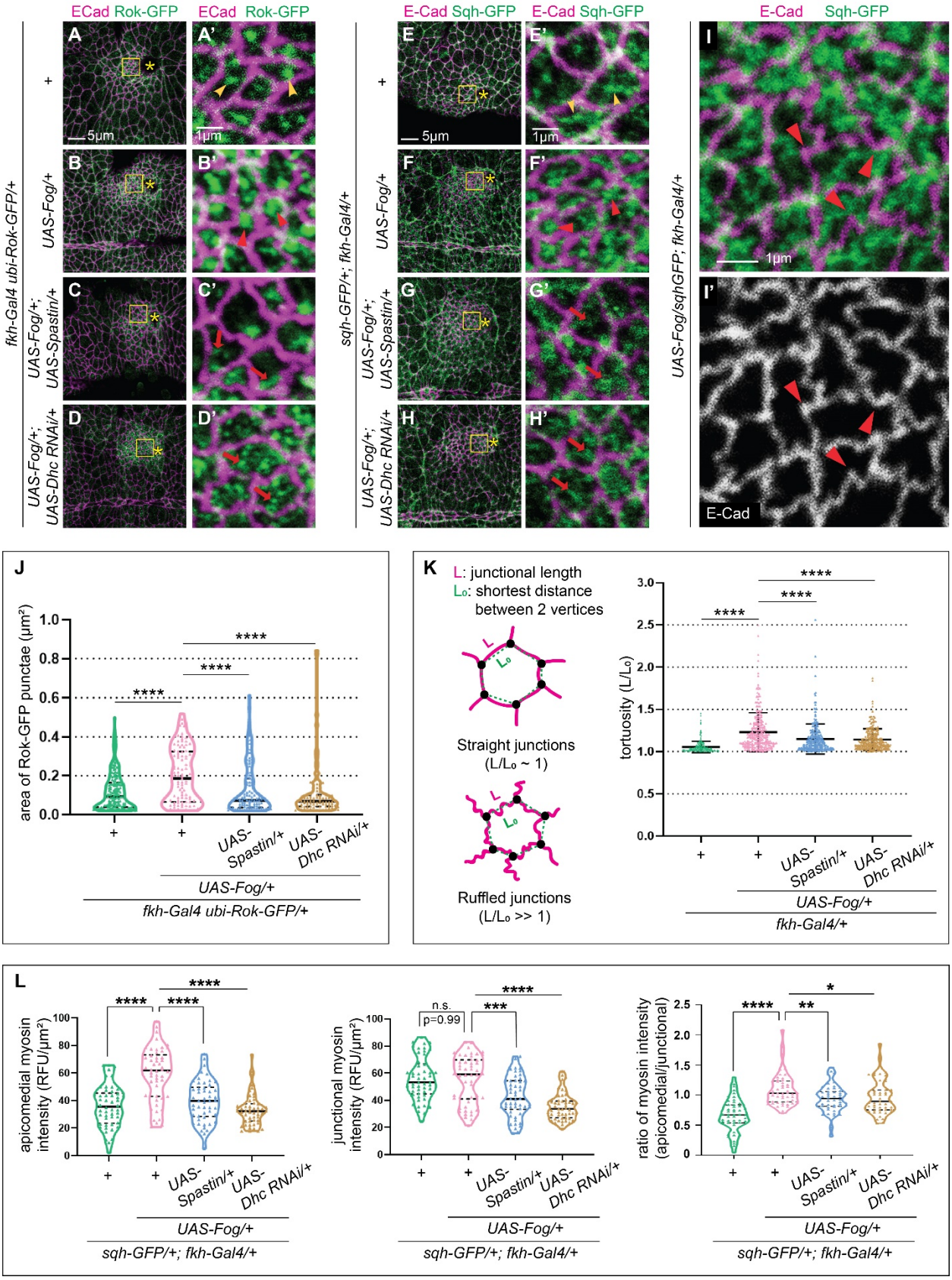
ECad Rok-GFP
ECad Rok-GFP
E-Cad Sqh-GFP
E-Cad Sqh-GFP
E-Cad
Sqh-GFP
fkh-Gal4 ubi-Rok-GFP/+
sqh-GFP/+; fkh-Gal4/+
UAS-Fog/sqhGFP; fkh-Gal4/+
UAS-Fog/+
UAS-Fog/+; UAS-Spastin/+
UAS-Fog/+; UAS-Dhc RNAi/+
5µm
1µm
E-Cad
area of Rok-GFP punctae (µm²)
L: junctional length
L₀: shortest distance between 2 vertices
Straight junctions (L/L₀ ~ 1)
Ruffled junctions (L/L₀ >> 1)
tortuosity (L/L₀)
apicomedial myosin intensity (RFU/µm²)
junctional myosin intensity (RFU/µm²)
ratio of myosin intensity (apicomedial/junctional)
n.s.
p=0.99
UAS-Spastin/+
UAS-Dhc RNAi/+
sqh-GFP/+; fkh-Gal4/+

673

674 **Fig. 7. Crb, E-Cad and Baz have a role in regulating apical constriction during SG**
675 **invagination.**

676 (A-C') Stage 11 SGs stained with Crb. (A'-C') Higher magnification of the yellow boxed
677 areas in A-C. Compared to control (A, A'), overexpression of Crb (B, B') results in
678 expansion of the apical membrane and accumulation of Crb on the cell surface (yellow
679 arrowheads). (C-C') Co-overexpression of spastin and Crb suppresses accumulation of
680 Crb. (D-G') Confocal images of SGs stained with E-Cad (D-G) and corresponding heat
681 maps for apical areas (D'-G'). (H) Percentage and cumulative percentage of cells with
682 different apical areas. Mann-Whitney U test (percentage of cells) and Kolmogorov-
683 Smirnov test (cumulative percentage of cells). n= 5 SGs (control, 517 cells; *Crb* RNAi,
684 583 cells; *E-Cad* RNAi, 712 cells; *Baz* RNAi, 601 cells). *, $p<0.05$. ****, $p<0.0001$.
685 Asterisks: invagination pit.

Figure 7

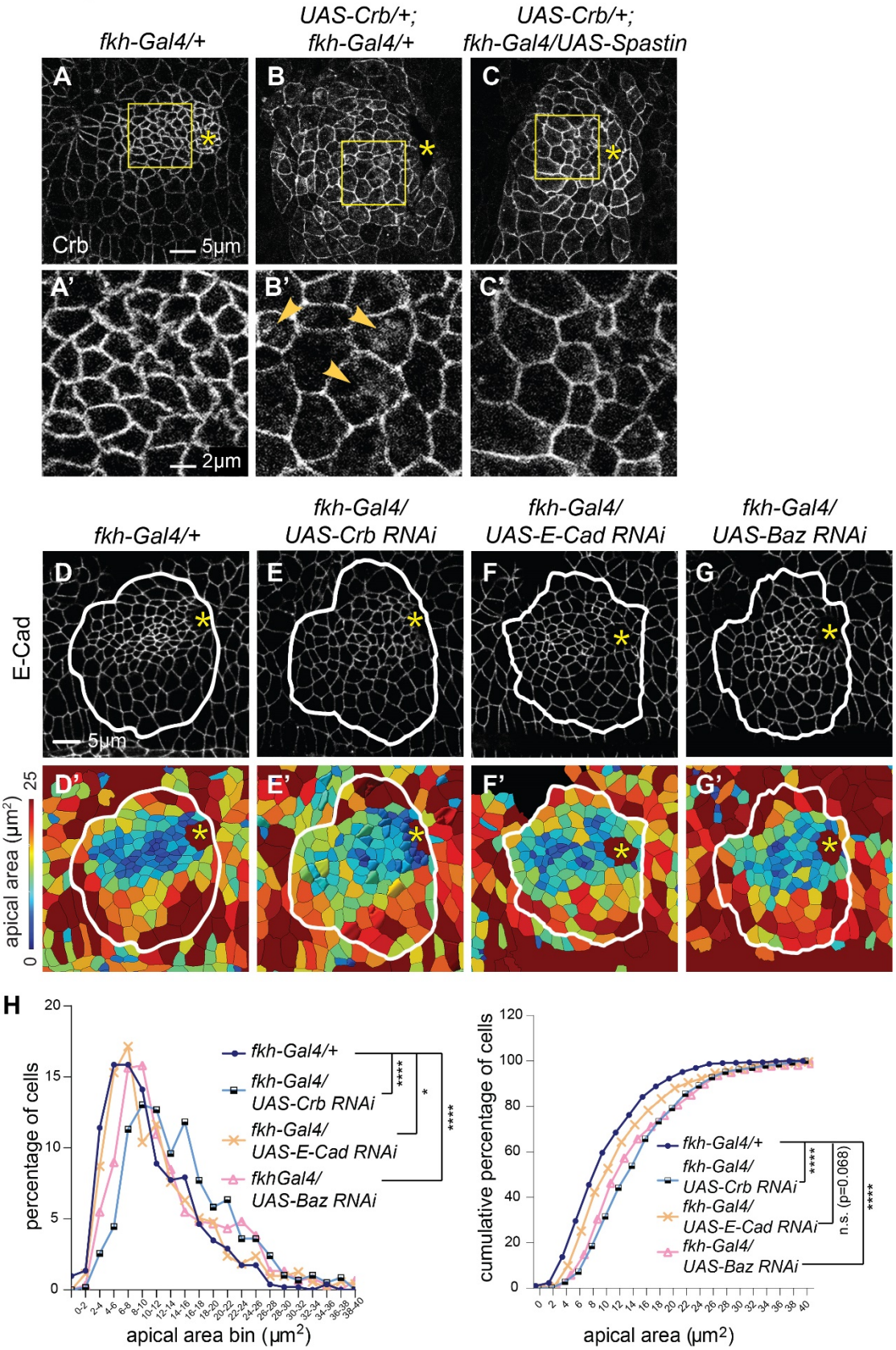
fkh-Gal4/+
UAS-Crb/+; fkh-Gal4/+
UAS-Crb/+; fkh-Gal4/UAS-Spastin
A
B
C
Crb
5µm
A'
B'
C'
2µm
fkh-Gal4/+
fkh-Gal4/ UAS-Crb RNAi
fkh-Gal4/ UAS-E-Cad RNAi
fkh-Gal4/ UAS-Baz RNAi
E-Cad
D
E
F
G
5µm
D'
E'
F'
G'
apical area (µm²)
25
0
H
percentage of cells
fkh-Gal4/+
fkh-Gal4/ UAS-Crb RNAi
fkh-Gal4/ UAS-E-Cad RNAi
fkhGal4/ UAS-Baz RNAi
****
*
****
apical area bin (µm²)
cumulative percentage of cells
n.s. (p=0.068)
apical area (µm²)

686

687 **Fig. 8. Knockdown of *crb*, *E-Cad* or *baz* results in reduced apicomedial myosin**
688 **formation and dispersed apicomedial Rok.** (A-D”) Compared to strong apicomedial
689 myosin in control SGs (yellow arrowheads in A’’), knockdown of *crb*, *E-Cad* or *baz* results
690 in reduction of apicomedial myosin in SG cells near the invagination pit (red arrowheads
691 in B’’-D’’). (A”-D”) Higher magnification of yellow boxed areas shown in A-D. (E)
692 Quantification of apicomedial myosin, junctional myosin and ratio of apicomedial to
693 junctional myosin of SG cells from different genotypes shown in A-D (n=5 SGs for each
694 genotype; 10 cells in the dorsal/ posterior region). **, p<0.01. ***, p< 0.001. ****, p<0.0001.
695 Mann-Whitney U test. (F-I’’) Compared to Rok accumulation in control SGs (yellow
696 arrowheads in F’’), reduction of *crb*, *E-Cad* or *baz* causes less accumulating Rok-GFP
697 signals in the apical domain of cells near the pit (red arrowheads in G’’-I’’). (F’’-I’’) Higher
698 magnification of yellow boxed areas shown in F-I. (J) Quantification of areas of Rok-GFP
699 puncta in SG cells from different genotypes shown in F-I (n=5 SGs; 15 cells in the
700 dorsal/posterior for each genotype). **, p< 0.01. ****, p< 0.0001. Mann-Whitney U test.
701 Asterisks: invagination pit.

Figure 8

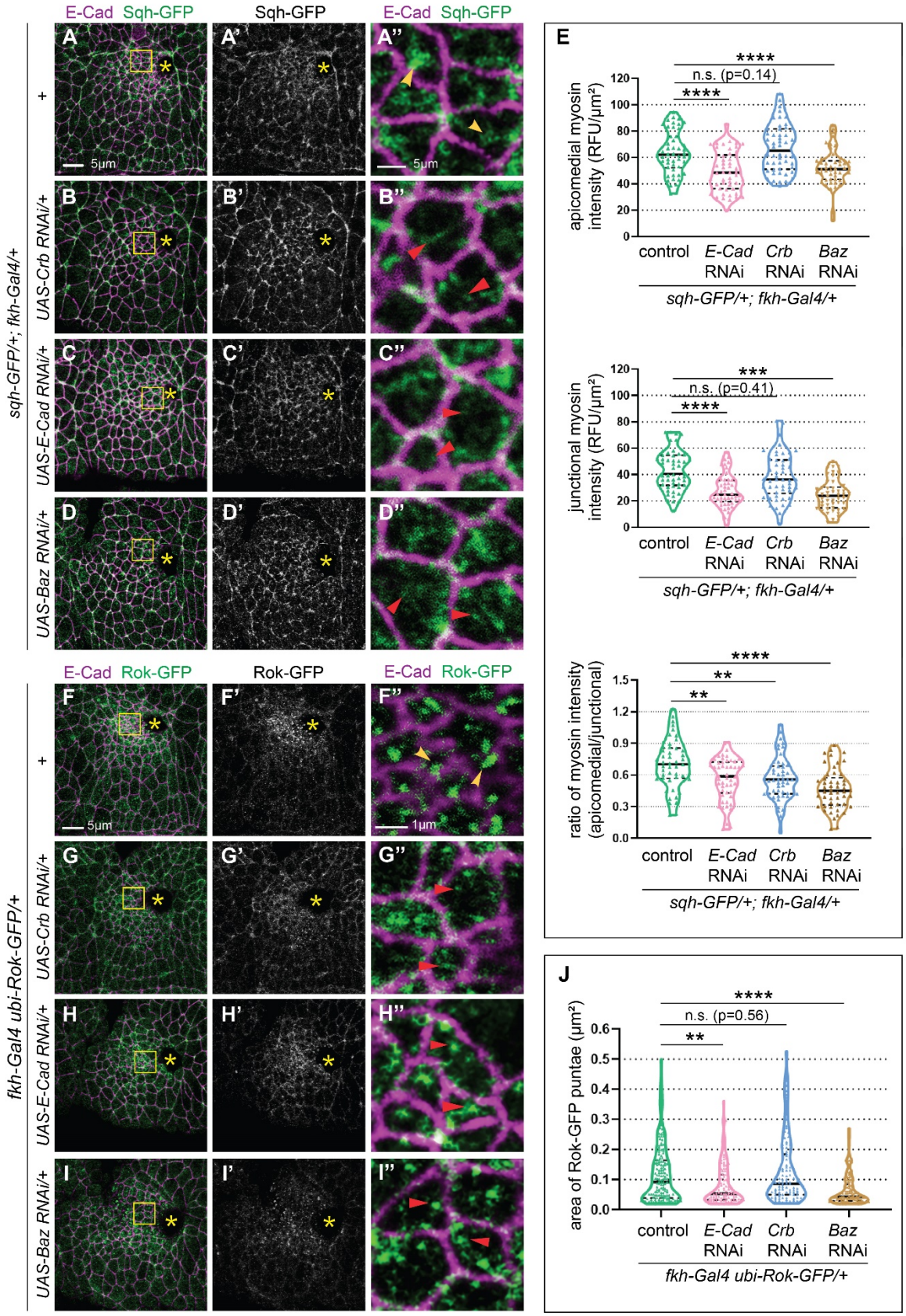
E-Cad Sqh-GFP
Sqh-GFP
E-Cad Sqh-GFP
A
A'
A''
B
B'
B''
C
C'
C''
D
D'
D''
5µm
sqh-GFP/+; fkh-Gal4/+
+
UAS-Crb RNAi/+
UAS-E-Cad RNAi/+
UAS-Baz RNAi/+
E-Cad Rok-GFP
Rok-GFP
E-Cad Rok-GFP
F
F'
F''
G
G'
G''
H
H'
H''
I
I'
I''
1µm
fkh-Gal4 ubi-Rok-GFP/+
E
apicomedial myosin intensity (RFU/µm²)
****
n.s. (p=0.14)
****
control
E-Cad RNAi
Crb RNAi
Baz RNAi
sqh-GFP/+; fkh-Gal4/+
junctional myosin intensity (RFU/µm²)
***
n.s. (p=0.41)
****
ratio of myosin intensity (apicomedial/junctional)
****
**
**
J
area of Rok-GFP puntae (µm²)
****
n.s. (p=0.56)
**
fkh-Gal4 ubi-Rok-GFP/+

703 **Fig. 9. MTs play a role in trafficking key apical and junctional proteins during SG**
704 **formation.**

705 (A-B’’’) Overexpression of spastin results in mislocalization of Rab11 and Nuf in stage 16
706 SGs. (A-A’’’) In control, Rab11 and Nuf localize in the apical region of SG cells (red
707 arrowheads). (B-B’’’) In spastin-overexpressing SGs, Rab11 and Nuf are mislocalized to
708 aggregates in the cytoplasm of cells (yellow arrowheads). (C-C’’’) Overexpression of Crb
709 causes mislocalization of Crb in all membrane domains and expands the membrane.
710 Rab11 is still enriched in the apical domain (red arrowheads). (D-D’’’) Co-overexpression
711 of spastin and Crb results in mislocalization of Crb to large aggregates in the cytoplasm,
712 which overlap with Rab11 (yellow arrowheads). (E-E’’’) Overexpression of E-Cad causes
713 a slight increase of the apical membrane, with the majority of E-Cad signals in the apical
714 domain (red arrowheads) and only some punctate E-Cad signals in the basolateral region
715 (blue arrows). (F-F’’’) Co-overexpression of E-Cad and spastin causes mislocalization of
716 E-Cad to cytoplasmic aggregates, which overlap with Nuf (yellow arrowheads). (G-G’’’)
717 Overexpression of Baz causes a slightly enlarged lumen. Red arrowheads, apical
718 localization of Baz and Nuf. (H-H’’’) The enlarged lumen phenotype caused by Baz
719 overexpression is suppressed when spastin is co-overexpressed. Blue arrows, a pool of
720 mislocalized Nuf overlaps with mislocalized Baz. Yellow arrowheads, mislocalized Nuf
721 that does not overlap with Baz. White dashed line, cell and nuclear boundaries (H) and
722 apical membrane (I). Nu, nucleus.

Figure 9

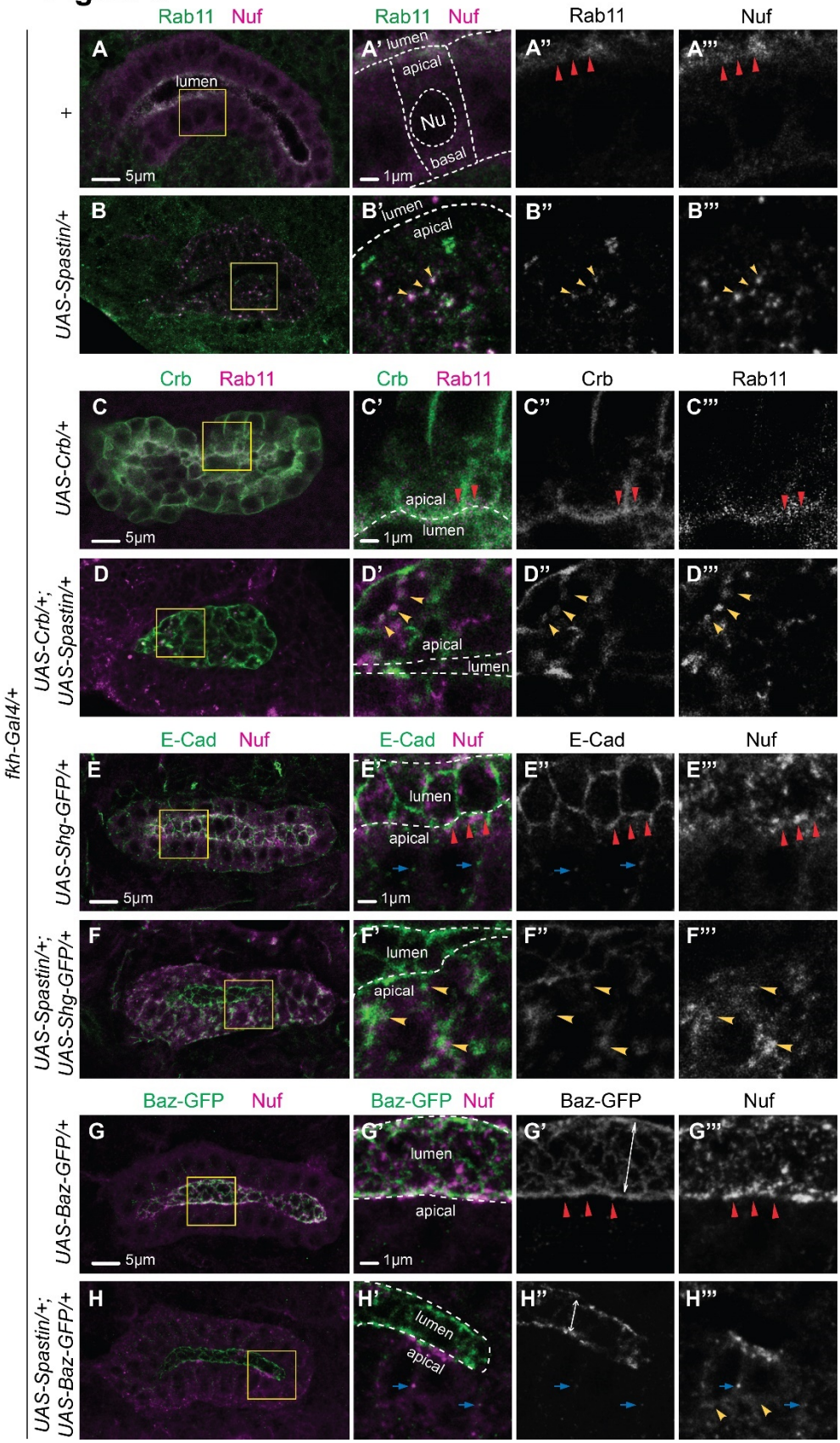
Rab11 Nuf
Rab11 Nuf
Rab11
Nuf
A
A'
A''
A'''
lumen
apical
Nu
basal
5μm
1μm
+
B
B'
B''
B'''
UAS-Spastin/+
Crb Rab11
Crb Rab11
Crb
Rab11
C
C'
C''
C'''
UAS-Crb/+
D
D'
D''
D'''
UAS-Crb/+;
UAS-Spastin/+
E-Cad Nuf
E-Cad Nuf
E-Cad
Nuf
E
E'
E''
E'''
UAS-Shg-GFP/+
F
F'
F''
F'''
UAS-Spastin/+;
UAS-Shg-GFP/+
Baz-GFP Nuf
Baz-GFP Nuf
Baz-GFP
Nuf
G
G'
G''
G'''
UAS-Baz-GFP/+
H
H'
H''
H'''
UAS-Spastin/+;
UAS-Baz-GFP/+
fkh-Gal4/+

723

724 **Fig. 10. A proposed model for MT-dependent trafficking to promote apical**
725 **constriction during SG invagination.** Vesicular transport is essential for apical
726 localization of Crb, E-Cad, and Baz to regulate apical myosin networks and subsequent
727 apical constriction. Fog signaling activity also depends on MTs and dynein motors.

728

729

730

Figure 10

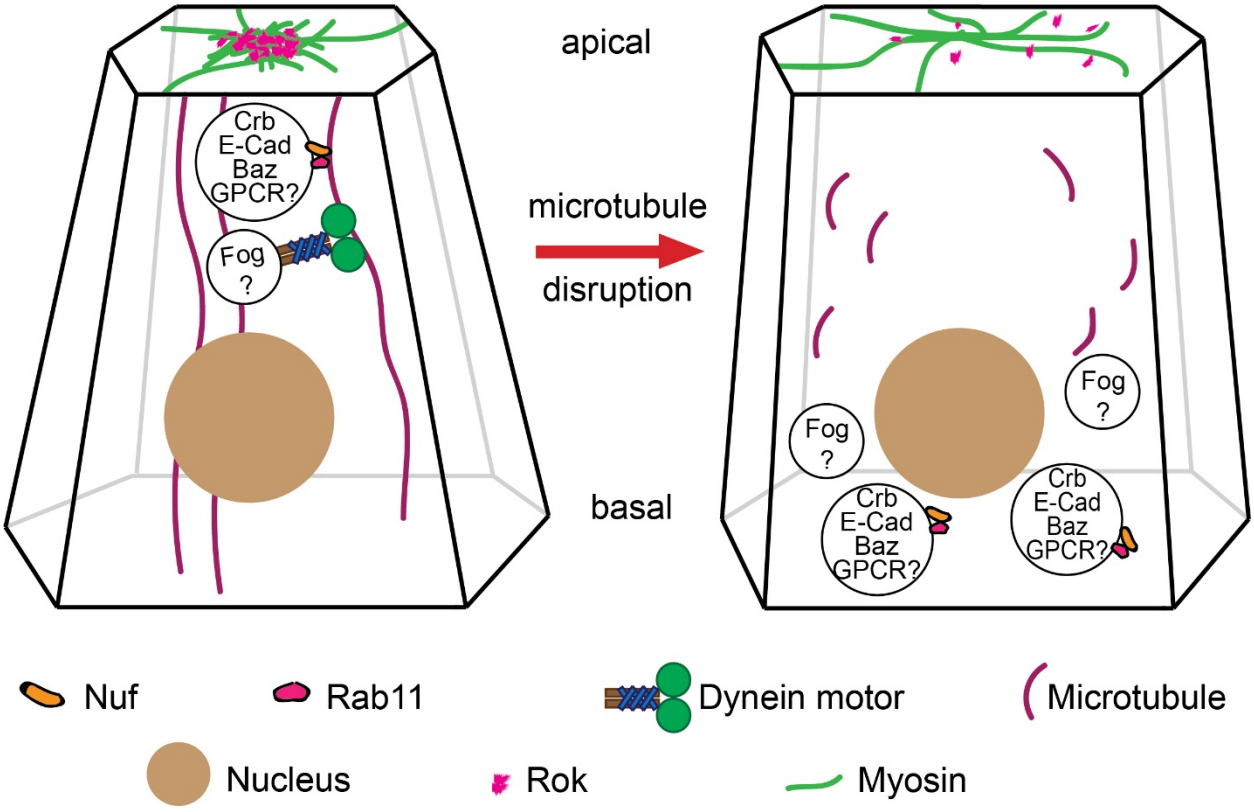

731

732

733 **Supplemental Fig. 1. Sec15 and Rab5-EYFP are enriched near the invagination pit**
734 **during SG invagination.** (A-B') Confocal images of a Rab5-EYFP SG stained with E-
735 Cad (A) and GFP (B). Rab5-EYFP signals are upregulated in the apical region near the
736 invagination pit. (A', B') Heat maps of apical areas (A') and intensity of Rab5-EYFP signals
737 (B'). Cells with small apical areas (dark blue cells in A') near the invagination pit show
738 high intensity of Rab5-EYFP (red cells in B'). (C) Negative correlation between Rab5-
739 EYFP intensity and apical areas of SG cells (n= 4 SGs; 396 cells). (D-E') Sec15 is
740 upregulated in the cells near the invagination pit. (D, E) Wild type embryo immunostained
741 with E-Cad and Sec15. (D', E') Heat maps of apical areas (D') and intensity of Sec15
742 signals (E'). (F) Negative correlation between intensity of Sec15 and apical areas of SG
743 cells (n= 5 SGs; 527 cells). Asterisks: invagination pit.

Supplemental Figure 1

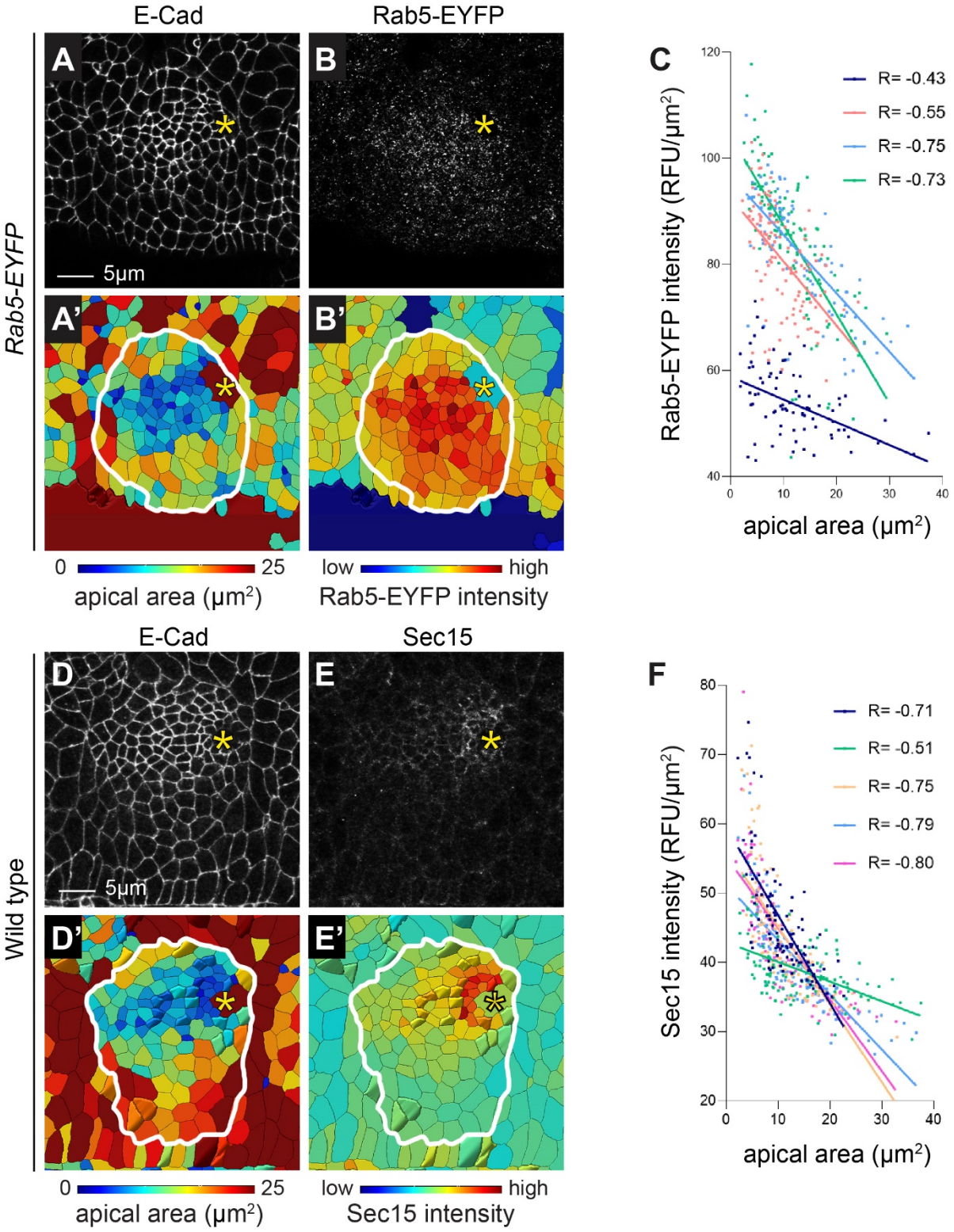

744

745 **Supplemental Fig. 2. Knockdown of *crb*, *E-Cad* and *baz* reduces Crb, E-Cad and**
746 **Baz levels in the SG.** (A-C'') Compared to strong Crb, E-Cad and Baz signals in control
747 SGs (A-C), knockdown of *crb*, *E-Cad* and *baz* results in reduction of Crb, E-Cad and Baz
748 levels in SG cells near the invagination pit (A'-C'). (A''-C'') Quantification of junctional
749 intensity of Crb, E-Cad and Baz. n=5 SGs (10 cells in the dorsal/posterior region of each
750 SG were tested). ****, $p < 0.0001$ (Mann-Whitney U test). Asterisks, invagination pit.

751

Supplemental Figure 2

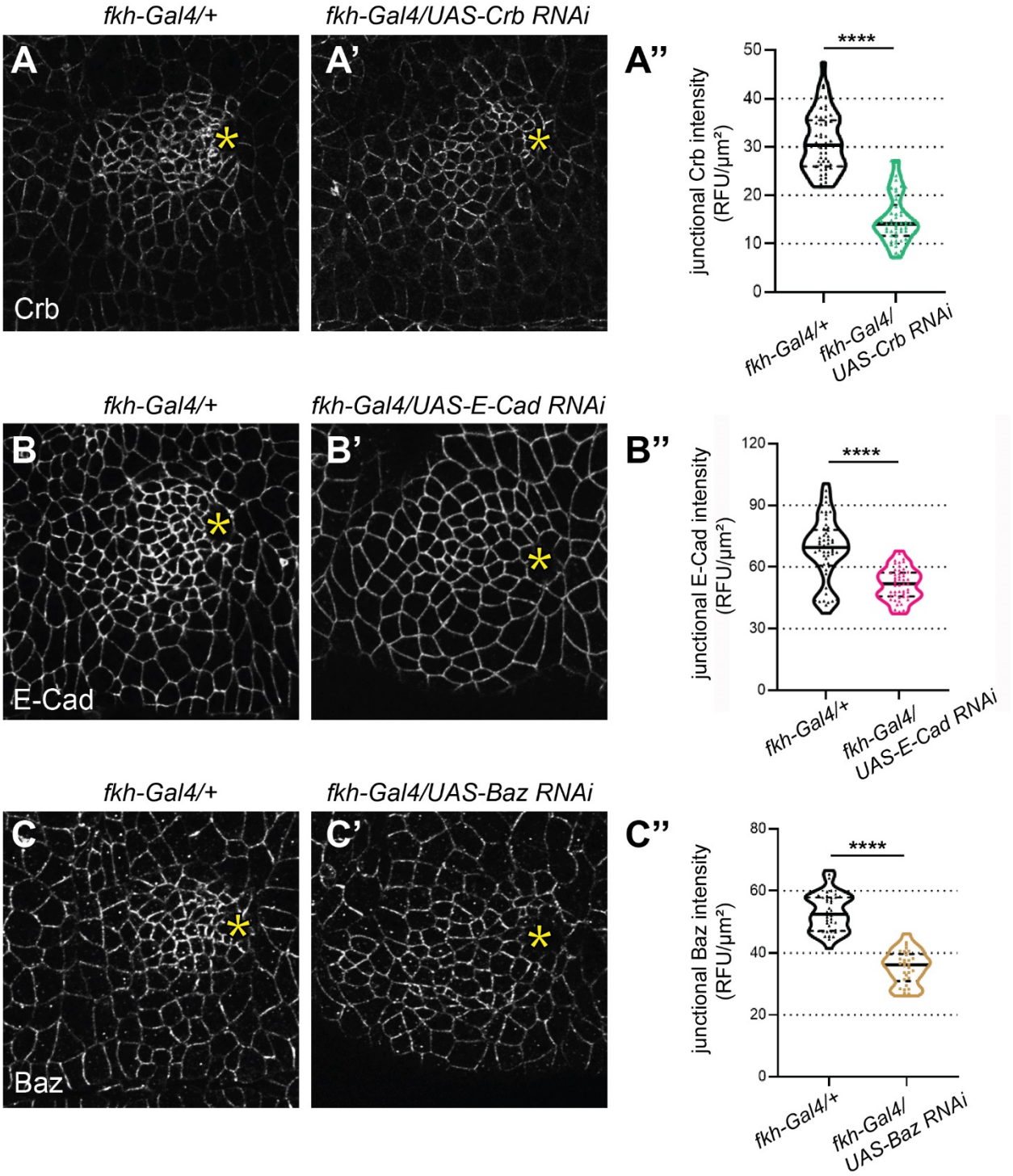

752

753

754 **Supplemental Fig. 3: Fog does not colocalize with Nuf when MTs are disrupted.** (A-
755 A''') A stage 16 SG overexpressing Fog shows mislocalized Fog as cytoplasmic
756 aggregates (yellow arrowheads). Nuf is still apically localized (red arrowheads). (B-B''')
757 When Fog and spastin are co-overexpressed, mislocalized Fog is mainly observed in the
758 basal region of cells. Nuf is mislocalized to the basolateral region of cells but does not
759 overlap with Fog (yellow arrowheads). Nu: nucleus.

760

761

Supplemental Figure 3

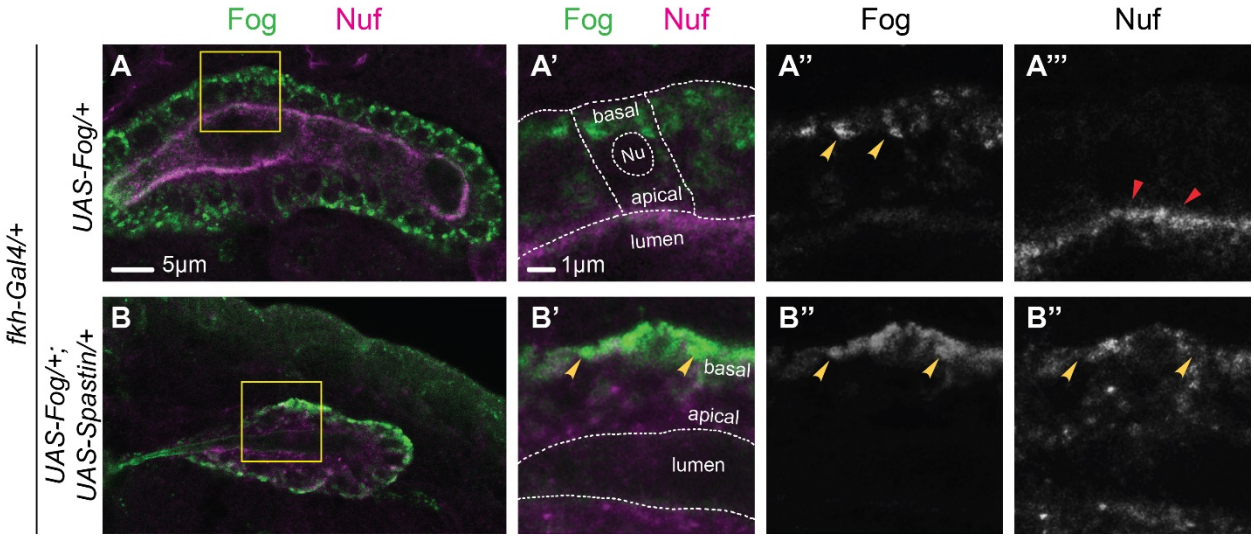

762

763

764

765 **Fly genotypes**

Figures	**Genotypes**
Figs. 1B-D', F-H', I-J'	Oregon R
Figs. 1K-L'	*Rab7-EYFP*
Figs. 2A-B''	Oregon R
Figs. 2D-D'''	*fkh-Gal4/+*
Figs. 2E-E''', F-G''	*fkh-Gal4/UAS-Spastin-CFP*
Figs. 3A-A'	*fkh-Gal4/+*
Figs. 3B-B'	*fkh-Gal4/UAS-Rab11-S25N-YFP*
Figs. 3C-C'	*UAS-Dicer-2/+; fkh-Gal4/UAS-Dhc64C RNAi*
Figs. 3D-D'	Oregon R
Figs. 3E-E'	*klar*^{1}
Fig. 3G, first left panel (top and bottom)	*fkh-Gal4/+*
Fig. 3G, three right panels (top and bottom)	*matα-Gal4/+; fkh-Gal4/UAS-Dhc64C RNAi*
Figs. 4A-A''''	*sqh-GFP/+; fkh-Gal4/+*
Figs. 4B-B''''	*sqh-GFP/UAS-Dicer-2; fkh-Gal4/UAS-Dhc64C RNAi*
Figs. 4D-D''''	*sqh-GFP; sqh*^{AX3}
Figs. 4E-E''''	*sqh-GFP; klar*^{1}
Figs. 5A-A''	*fkh-Gal4 ubi-Rok-GFP/+*

Figs. 5B-B''	*UAS-Spastin; fkh-Gal4 ubi-Rok-GFP/+*
Figs. 5C-C''	*UAS-Dicer-2/+; fkh-Gal4 ubi-Rok-GFP/UAS-Dhc64C RNAi*
Figs. 5D-D''	*ubi-Rok-GFP*
Figs. 5E-E''	*klarmCD4 ubi-Rok-GFP*
Figs. 5F	*fkh-Gal4 ubi-Rok-GFP/+*
Figs. 6A-A'	*fkh-Gal4 ubi-Rok-GFP/+*
Figs. 6B-B'	*UAS-Fog/+; fkh-Gal4 ubi-Rok-GFP/+*
Figs. 6C-C'	*UAS-Fog/+; fkh-Gal4 ubi-Rok-GFP/UAS-Spastin*
Figs. 6D-D'	*UAS-Fog/+; fkh-Gal4 ubi-Rok-GFP/UAS-Dhc64C RNAi*
Figs. 6E-E'	*sqh-GFP/+; fkh-Gal4/+*
Figs. 6F-F'	*sqh-GFP/UAS-Fog; fkh-Gal4/+*
Figs. 6G-G'	*sqh-GFP/UAS-Fog; fkh-Gal4/UAS-Spastin*
Figs. 6H-H'	*sqh-GFP/UAS-Fog; fkh-Gal4/UAS-Dhc64C RNAi*
Figs. 6I-I'	*sqh-GFP/UAS-Fog; fkh-Gal4/+*
Figs. 7A-A'	*fkh-Gal4/+*
Figs. 7B-B'	*UAS-Crb/+; fkh-Gal4/+*
Figs. 7C-C'	*UAS-Crb/+; fkh-Gal4/UAS-Spastin*

Figs. 7D-D’	*fkh-Gal4/+*
Figs. 7E-E’	*fkh-Gal4/UAS-Crb RNAi*
Figs. 7F-F’	*fkh-Gal4/UAS-E-Cad RNAi*
Figs. 7G-G’	*fkh-Gal4/UAS-Baz RNAi*
Figs. 8A-A’’	*sqh-GFP/+; fkh-Gal4/+*
Figs. 8B-B’’	*sqh-GFP/+; fkh-Gal4/UAS-Crb RNAi*
Figs. 8C-C’’	*sqh-GFP/+; fkh-Gal4/UAS-E-Cad RNAi*
Figs. 8D-D’’	*sqh-GFP/+; fkh-Gal4/UAS-Baz RNAi*
Figs. 8F-F’’	*fkh-Gal4 ubi-Rok-GFP/+*
Figs. 8G-G’’	*fkh-Gal4 ubi-Rok-GFP/UAS-Crb RNAi*
Figs. 8H-H’’	*fkh-Gal4 ubi-Rok-GFP/UAS-E-Cad RNAi*
Figs. 8I-I’’	*fkh-Gal4 ubi-Rok-GFP/UAS-Baz RNAi*
Figs. 9A-A’’’	*fkh-Gal4/+*
Figs. 9B-B’’’	*fkh-Gal4/UAS-Spastin*
Figs. 9C-C’’’	*UAS-Crb/+; fkh-Gal4/+*
Figs. 9D’D’’’	*UAS-Crb/+; fkh-Gal4/UAS-Spastin*
Figs. 9E-E’’’	*fkh-Gal4/UAS-Shg-GFP*
Figs. 9F-F’’’	*UAS-Spastin/+; fkh-Gal4/UAS-Shg-GFP*
Figs. 9G-G’’’	*fkh-Gal4/UAS-Baz-GFP*

Figs. 9H-H’’’	*UAS-Spastin/+; fkh-Gal4/UAS-Baz-GFP*
Sup. Figs. 1A-B’	*Rab5-EYFP*
Sup. Figs. 1D-E’	Oregon R
Sup. Figs. 2A,B,C	*fkh-Gal4/+*
Sup. Fig. 2A’	*fkh-Gal4/UAS-Crb* RNAi
Sup. Fig. 2B’	*fkh-Gal4/UAS-E-Cad* RNAi
Sup. Fig. 2C’	*fkh-Gal4/UAS-Baz* RNAi
Sup. Figs. 3A-A’’’	*UAS-Fog/+; fkh-Gal4/+*
Sup. Figs. 3B-B’’’	*UAS-Fog/+; fkh-Gal4/UAS-Spastin*

766

767

768

769

770 **References**

771 Aguilar-Aragon, M., G. Fletcher and B. J. Thompson (2019). Apical transport of Crumbs
772 maintains epithelial cell polarity. Biorxiv.
773 Anborgh, P.H., Seachrist, J.L., Dale, L.B., and Ferguson, S.S. (2000). Receptor/beta-arrestin
774 complex formation and the differential trafficking and resensitization of beta2-adrenergic and
775 angiotensin II type 1A receptors. Mol Endocrinol *14*, 2040-2053.
776 Andrew, D.J., and Ewald, A.J. (2010). Morphogenesis of epithelial tubes: Insights into tube
777 formation, elongation, and elaboration. Dev Biol *341*, 34-55.
778 Benton, M.A., Frey, N., Nunes da Fonseca, R., von Levetzow, C., Stappert, D., Hakeemi, M.S.,
779 Conrads, K.H., Pechmann, M., Panfilio, K.A., Lynch, J.A., *et al.* (2019). Fog signaling has
780 diverse roles in epithelial morphogenesis in insects. Elife *8*.
781 Benton, R., and St Johnston, D. (2003). Drosophila PAR-1 and 14-3-3 inhibit Bazooka/PAR-3 to
782 establish complementary cortical domains in polarized cells. Cell *115*, 691-704.
783 Booth, A.J.R., Blanchard, G.B., Adams, R.J., and Roper, K. (2014). A dynamic microtubule
784 cytoskeleton directs medial actomyosin function during tube formation. Dev Cell *29*, 562-576.
785 Cerniello, F.M., Carretero, O.A., Longo Carbajosa, N.A., Cerrato, B.D., Santos, R.A., Grecco,
786 H.E., and Gironacci, M.M. (2017). MAS1 Receptor Trafficking Involves ERK1/2 Activation
787 Through a beta-Arrestin2-Dependent Pathway. Hypertension *70*, 982-989.
788 Chung, S., and Andrew, D.J. (2014). Cadherin 99C regulates apical expansion and cell
789 rearrangement during epithelial tube elongation. Development *141*, 1950-1960.
790 Chung, S., Hanlon, C.D., and Andrew, D.J. (2014). Building and specializing epithelial tubular
791 organs: the Drosophila salivary gland as a model system for revealing how epithelial organs are
792 specified, form and specialize. Wiley Interdiscip Rev Dev Biol *3*, 281-300.
793 Chung, S., Kim, S., and Andrew, D.J. (2017). Uncoupling apical constriction from tissue
794 invagination. Elife *6*.
795 Dale, L.B., Seachrist, J.L., Babwah, A.V., and Ferguson, S.S. (2004). Regulation of angiotensin
796 II type 1A receptor intracellular retention, degradation, and recycling by Rab5, Rab7, and Rab11
797 GTPases. J Biol Chem *279*, 13110-13118.
798 David, D.J., Tishkina, A., and Harris, T.J. (2010). The PAR complex regulates pulsed
799 actomyosin contractions during amnioserosa apical constriction in Drosophila. Development
800 *137*, 1645-1655.
801 Fan, G.H., Lapierre, L.A., Goldenring, J.R., and Richmond, A. (2003). Differential regulation of
802 CXCR2 trafficking by Rab GTPases. Blood *101*, 2115-2124.
803 Fuse, N., Yu, F., and Hirose, S. (2013). Gprk2 adjusts Fog signaling to organize cell movements
804 in Drosophila gastrulation. Development *140*, 4246-4255.
805 Gorvel, J.P., Chavrier, P., Zerial, M., and Gruenberg, J. (1991). rab5 controls early endosome
806 fusion in vitro. Cell *64*, 915-925.
807 Gross, S.P., Welte, M.A., Block, S.M., and Wieschaus, E.F. (2000). Dynein-mediated cargo
808 transport in vivo. A switch controls travel distance. J Cell Biol *148*, 945-956.
809 Guglielmi, G., Barry, J.D., Huber, W., and De Renzis, S. (2015). An Optogenetic Method to
810 Modulate Cell Contractility during Tissue Morphogenesis. Dev Cell *35*, 646-660.
811 Hamelin, E., Theriault, C., Laroche, G., and Parent, J.L. (2005). The intracellular trafficking of
812 the G protein-coupled receptor TPbeta depends on a direct interaction with Rab11. J Biol Chem
813 *280*, 36195-36205.

814 Hunyady, L., Baukal, A.J., Gaborik, Z., Olivares-Reyes, J.A., Bor, M., Szaszak, M., Lodge, R.,
815 Catt, K.J., and Balla, T. (2002). Differential PI 3-kinase dependence of early and late phases of
816 recycling of the internalized AT1 angiotensin receptor. J Cell Biol *157*, 1211-1222.
817 Innamorati, G., Le Gouill, C., Balamotis, M., and Birnbaumer, M. (2001). The long and the short
818 cycle. Alternative intracellular routes for trafficking of G-protein-coupled receptors. J Biol Chem
819 *276*, 13096-13103.
820 Izquierdo, E., Quinkler, T., and De Renzis, S. (2018). Guided morphogenesis through
821 optogenetic activation of Rho signalling during early Drosophila embryogenesis. Nat Commun
822 *9*, 2366.
823 Jouette, J., Guichet, A., and Claret, S.B. (2019). Dynein-mediated transport and membrane
824 trafficking control PAR3 polarised distribution. Elife *8*.
825 Kerridge, S., Munjal, A., Philippe, J.M., Jha, A., de las Bayonas, A.G., Saurin, A.J., and Lecuit,
826 T. (2016). Modular activation of Rho1 by GPCR signalling imparts polarized myosin II
827 activation during morphogenesis. Nat Cell Biol *18*, 261-270.
828 Khanal, I., Elbediwy, A., Diaz de la Loza Mdel, C., Fletcher, G.C., and Thompson, B.J. (2016).
829 Shot and Patronin polarise microtubules to direct membrane traffic and biogenesis of microvilli
830 in epithelia. J Cell Sci *129*, 2651-2659.
831 Ko, C.S., Tserunyan, V., and Martin, A.C. (2019). Microtubules promote intercellular contractile
832 force transmission during tissue folding. J Cell Biol *218*, 2726-2742.
833 Laan, L., Pavin, N., Husson, J., Romet-Lemonne, G., van Duijn, M., Lopez, M.P., Vale, R.D.,
834 Julicher, F., Reck-Peterson, S.L., and Dogterom, M. (2012). Cortical dynein controls
835 microtubule dynamics to generate pulling forces that position microtubule asters. Cell *148*, 502-
836 514.
837 Langevin, J., Morgan, M.J., Sibarita, J.B., Aresta, S., Murthy, M., Schwarz, T., Camonis, J., and
838 Bellaiche, Y. (2005). Drosophila exocyst components Sec5, Sec6, and Sec15 regulate DE-
839 Cadherin trafficking from recycling endosomes to the plasma membrane. Dev Cell *9*, 365-376.
840 Le Droguen, P.M., Claret, S., Guichet, A., and Brodu, V. (2015). Microtubule-dependent apical
841 restriction of recycling endosomes sustains adherens junctions during morphogenesis of the
842 Drosophila tracheal system. Development *142*, 363-374.
843 Lee, J.Y., and Harland, R.M. (2010). Endocytosis is required for efficient apical constriction
844 during Xenopus gastrulation. Curr Biol *20*, 253-258.
845 Letizia, A., Sotillos, S., Campuzano, S., and Llimargas, M. (2011). Regulated Crb accumulation
846 controls apical constriction and invagination in Drosophila tracheal cells. J Cell Sci *124*, 240-
847 251.
848 Li, M., McGrail, M., Serr, M., and Hays, T.S. (1994). Drosophila cytoplasmic dynein, a
849 microtubule motor that is asymmetrically localized in the oocyte. J Cell Biol *126*, 1475-1494.
850 Manning, A.J., Peters, K.A., Peifer, M., and Rogers, S.L. (2013). Regulation of epithelial
851 morphogenesis by the G protein-coupled receptor mist and its ligand fog. Sci Signal *6*, ra98.
852 Manning, A.J., and Rogers, S.L. (2014). The Fog signaling pathway: insights into signaling in
853 morphogenesis. Dev Biol *394*, 6-14.
854 Martin, A.C., and Goldstein, B. (2014). Apical constriction: themes and variations on a cellular
855 mechanism driving morphogenesis. Development *141*, 1987-1998.
856 Martin, A.C., Kaschube, M., and Wieschaus, E.F. (2009). Pulsed contractions of an actin-myosin
857 network drive apical constriction. Nature *457*, 495-499.
858 Mason, F.M., Tworoger, M., and Martin, A.C. (2013). Apical domain polarization localizes
859 actin-myosin activity to drive ratchet-like apical constriction. Nat Cell Biol *15*, 926-936.

860 Meresse, S., Gorvel, J.P., and Chavrier, P. (1995). The rab7 GTPase resides on a vesicular
861 compartment connected to lysosomes. J Cell Sci *108 (Pt 11)*, 3349-3358.
862 Miao, H., Vanderleest, T.E., Jewett, C.E., Loerke, D., and Blankenship, J.T. (2019). Cell
863 ratcheting through the Sbf RabGEF directs force balancing and stepped apical constriction. J Cell
864 Biol.
865 Myat, M.M., and Andrew, D.J. (2000). Organ shape in the Drosophila salivary gland is
866 controlled by regulated, sequential internalization of the primordia. Development *127*, 679-691.
867 Myat, M.M., and Andrew, D.J. (2002). Epithelial tube morphology is determined by the
868 polarized growth and delivery of apical membrane. Cell *111*, 879-891.
869 Ossipova, O., Kim, K., Lake, B.B., Itoh, K., Ioannou, A., and Sokol, S.Y. (2014). Role of Rab11
870 in planar cell polarity and apical constriction during vertebrate neural tube closure. Nat Commun
871 *5*, 3734.
872 Rauzi, M., Lenne, P.F., and Lecuit, T. (2010). Planar polarized actomyosin contractile flows
873 control epithelial junction remodelling. Nature *468*, 1110-1114.
874 Riggs, B., Rothwell, W., Mische, S., Hickson, G.R., Matheson, J., Hays, T.S., Gould, G.W., and
875 Sullivan, W. (2003). Actin cytoskeleton remodeling during early Drosophila furrow formation
876 requires recycling endosomal components Nuclear-fallout and Rab11. J Cell Biol *163*, 143-154.
877 Roeth, J.F., Sawyer, J.K., Wilner, D.A., and Peifer, M. (2009). Rab11 helps maintain apical
878 crumbs and adherens junctions in the Drosophila embryonic ectoderm. PLoS One *4*, e7634.
879 Roper, K. (2012). Anisotropy of Crumbs and aPKC drives myosin cable assembly during tube
880 formation. Dev Cell *23*, 939-953.
881 Royou, A., Field, C., Sisson, J.C., Sullivan, W., and Karess, R. (2004). Reassessing the role and
882 dynamics of nonmuscle myosin II during furrow formation in early Drosophila embryos. Mol
883 Biol Cell *15*, 838-850.
884 Sanchez-Corrales, Y.E., Blanchard, G.B., and Roper, K. (2018). Radially patterned cell
885 behaviours during tube budding from an epithelium. Elife *7*.
886 Sawyer, J.M., Harrell, J.R., Shemer, G., Sullivan-Brown, J., Roh-Johnson, M., and Goldstein, B.
887 (2010). Apical constriction: a cell shape change that can drive morphogenesis. Dev Biol *341*, 5-
888 19.
889 Sherwood, N.T., Sun, Q., Xue, M., Zhang, B., and Zinn, K. (2004). Drosophila spastin regulates
890 synaptic microtubule networks and is required for normal motor function. PLoS Biol *2*, e429.
891 Sidor, C., Stevens, T.J., Jin, L., Boulanger, J., and Roper, K. (2020). Rho-Kinase Planar
892 Polarization at Tissue Boundaries Depends on Phospho-regulation of Membrane Residence
893 Time. Dev Cell *52*, 364-378 e367.
894 Ullrich, O., Reinsch, S., Urbe, S., Zerial, M., and Parton, R.G. (1996). Rab11 regulates recycling
895 through the pericentriolar recycling endosome. J Cell Biol *135*, 913-924.
896 Urbansky, S., Gonzalez Avalos, P., Wosch, M., and Lemke, S. (2016). Folded gastrulation and
897 T48 drive the evolution of coordinated mesoderm internalization in flies. Elife *5*.
898 Volpicelli, L.A., Lah, J.J., Fang, G., Goldenring, J.R., and Levey, A.I. (2002). Rab11a and
899 myosin Vb regulate recycling of the M4 muscarinic acetylcholine receptor. J Neurosci *22*, 9776-
900 9784.
901 Westermann, S., and Weber, K. (2003). Post-translational modifications regulate microtubule
902 function. Nat Rev Mol Cell Biol *4*, 938-947.
903 Wichmann, H., Hengst, L., and Gallwitz, D. (1992). Endocytosis in yeast: evidence for the
904 involvement of a small GTP-binding protein (Ypt7p). Cell *71*, 1131-1142.

905 Wodarz, A., Grawe, F., and Knust, E. (1993). CRUMBS is involved in the control of apical
906 protein targeting during Drosophila epithelial development. Mech Dev *44*, 175-187.
907 Yvon, A.M., Gross, D.J., and Wadsworth, P. (2001). Antagonistic forces generated by myosin II
908 and cytoplasmic dynein regulate microtubule turnover, movement, and organization in interphase
909 cells. Proc Natl Acad Sci U S A *98*, 8656-8661.
910 Zhang, X.M., Ellis, S., Sriratana, A., Mitchell, C.A., and Rowe, T. (2004). Sec15 is an effector
911 for the Rab11 GTPase in mammalian cells. J Biol Chem *279*, 43027-43034.

912